Geomorphology 400 (2022) 108095

Contents lists available at ScienceDirect

Geomorphology

journal homepage: www.elsevier.com/locate/geomorph

Age attribution to a karst system using river long profile analysis (Hyblean Plateau, Sicily, Italy)

F. Pavano [a,*], G. Tortorici [b], G. Romagnoli [c,d], S. Catalano [b,c]

[a] Department of Earth and Environmental Sciences, Lehigh University, Bethlehem, PA, USA
[b] Department of Biological, Geological and Environmental Sciences, University of Catania, Catania, Italy
[c] Consiglio Nazionale delle Ricerche, Istituto di Geologia Ambientale e Geoingegneria, Montelibretti, Rome, Italy
[d] Istituto Superiore per la Protezione e la Ricerca Ambientale, Servizio Geologico d'Italia, Rome, Italy

ARTICLE INFO

Article history:
Received 30 April 2021
Received in revised form 20 December 2021
Accepted 24 December 2021
Available online 31 December 2021

Keywords:
Hyblean Plateau
Cassibile River
Long profile
Karst caves

ABSTRACT

In steady-state tectonic-climate systems, the fluvio-karst processes attain a stable base level, whether it be local or global. In contrast, in an uplifting region, relative base-level changes force river incision processes and a concurrent lowering of the karst water-table. Even at local scales (e.g., single fault-controlled valley), combined tectonically- and climatically-driven base-level drops induce geomorphic and hydrogeological disequilibrium. Thus, the karst system develops vertically and the water-table lowers trying to attain the new local base level. Conversely, the paleo-karst network dries, and becomes abandoned as a hanging relic with aligned karst morphologies. They are exhumed by the entrenchment of the fluvial network, as base-level fall related knickpoints migrate upstream. We propose a geomorphic approach to build fluvio-karst age models, based upon the analysis of river long-profiles. This approach is complementary to altimetric correlation between karst horizons and coastal paleo-sea level markers. Our approach is useful for an inland study area that is far from the marine terraced coast or where active faulting cuts off the coastal area from the inland landscape. We tested the approach in the eastern sector of the Hyblean Plateau (Sicily, Italy), where a carbonate sequence experienced Middle-Late Pleistocene tectonic uplift combined with active faulting. Specifically, we investigated the Cassibile River basin, at the footwall of the active Cassibile-Noto Fault. By reconstructing river paleo-long profiles we fixed time-space reference lines, connecting the abandoned and hanging fluvio-karst levels to the correlative marine strandlines carved along the fault-controlled coastal landscape.

1. Introduction

Dating the beginning and the evolution of karst systems is one of the main targets of speleologists and researchers of karst processes. Previous studies carried out in carbonate bedrock settings suggest that karst cave initiation is rapid and in the order of ≤100 kyr, whereas the development of a complete surface and subsurface karst system needs hundreds of thousands of years (White, 1988; Palmer, 1991; Korpas, 1998; Dreybrodt and Gabrovšek, 2000; Granger et al., 2001; Bosak, 2002). Karst system-related processes (e.g. karst widening and deepening; karst infilling with sediment; karst conduit speleothem development) often depend on changes in base level (Ford and Williams, 2007). These changes can result from a combination of climatic cycles (e.g. glacial-interglacial alternation) and vertical crustal motions (e.g., Westaway, 1993; Bosi et al., 1996; Tortorici et al., 2003; Catalano et al., 2008b; Canora et al., 2012; Columbu et al., 2017; Meschis et al., 2020). The age determinations for karst processes and their related morphologies are commonly based on bio- and geochronological dating of the infilling sediments and speleothems in karst caves and conduits (White, 1988; Ford and Williams, 1989; Geyh and Schleicher, 1990; Colman and Pierce, 2000; Dumitru, 2000; Forman et al., 2000; Noller et al., 2000; Bosak, 2002; Meyer et al., 2011; Szanyi et al., 2012; Audra and Palmer, 2013; Hauselmann et al., 2015; Columbu et al., 2017; Engel et al., 2020; Dumitru et al., 2021). For karst systems lacking direct geochronological constraints, alternative indirect dating methods are often based on either the correlation of karst morphologies with independently dated fluvial (Hromas, 1968; Harmand et al., 2017) or marine (e.g., Florea and Vacher, 2006; Canora et al., 2012) terraces. These indirect methods imply short distance and/or a physical continuity between the fluvial or karst forms and the coastal area, where the signals of Quaternary eustatic oscillations are morphologically expressed as marine terraces and paleo-shorelines.

However, the larger the distance from the coastal areas, the larger the uncertainties for any direct lateral correlations. These correlations

* Corresponding author.
E-mail address: frp319@lehigh.edu (F. Pavano).

https://doi.org/10.1016/j.geomorph.2021.108095
0169-555X/

can be further problematic due to active tectonics which can deform the primary geometry of the marine terrace features of the coastal belt and the correlative fluvial landforms of the inland continental landscape (Catalano et al., 2003; Tortorici et al., 2003; Pavano et al., 2015). In this situation, correlations simply based on the altimetry of landforms can be unreliable, with the reconstruction of almost continuous dated reference morphological levels being required. Along the coast, marine strandlines provide good, dated reference levels to depict both cumulative uplift and deformation (Catalano and De Guidi, 2003; De Guidi et al., 2003; Catalano et al., 2008a). River long profile reconstruction (e.g., Gallen et al., 2013; Regalla et al., 2013; Pavano et al., 2016; Castillo et al., 2017) is a powerful and reliable method for connecting these sea level markers to their correlative fluvial levels of the inland continental landscape. The combined use of marine strandlines and river long profiles could thus provide a 2D framework of almost continuous dated space-time reference lines, allowing for the indirect dating of paleo-karst levels both along the coast as well as inland. We demonstrate this approach for dating abandoned and exhumed fluvio-karst horizons in the south-eastern sectors of the Hyblean Plateau region (SE Sicily, Italy). Our study area extends across two adjacent sites, the Floridia Basin and the Cassibile River canyon (Fig. 1). These two sectors show different morphological settings, allowing linkage of the paleo-karst features with marine and fluvial landforms. In the Floridia Basin, geochronological data, coupled with the lateral continuity of almost undisturbed marine strandlines, are sufficient to reconstruct an age-model based on altimetric correlation of the landforms. The Cassibile River canyon refers to an actively deforming region, which is located at the footwall of the Cassibile-Noto normal fault (Bianca et al., 1999; Catalano et al., 2008b, 2010; Pavano et al., 2019) (Fig. 1). In this area, we take advantage of the reconstruction of river long-profiles, shaped by the retreat of knickpoints, as a tool to obtain hypothetical reference lines that connect fluvial features to downstream sea level markers (in the range of 10^0–10^2 km; Crosby and Whipple, 2006; Kirby and Whipple, 2012; Gallen et al., 2013; Pavano et al., 2016; Jaiswara et al., 2019). In order to rule out any connection between the knickpoints locations and the occurrence of faults, we explore their relative spatial distribution. The analyzed knickpoints are transient, upstream-migrating geomorphic expressions of base-level lowering events along the coast (Howard, 1994; Kirby and Whipple, 2001; Wegmann and Pazzaglia, 2002; Bishop et al., 2005; Crosby and Whipple, 2006; Wobus et al., 2006; Brocard et al., 2016; Pavano et al., 2016; Robustelli, 2019; Boulton, 2020; Bhattarai et al., 2021; Pavano and Gallen, 2021), recorded by the difference in elevation between marine strandlines of successive eustatic highstands. The correlation between the knickpoints

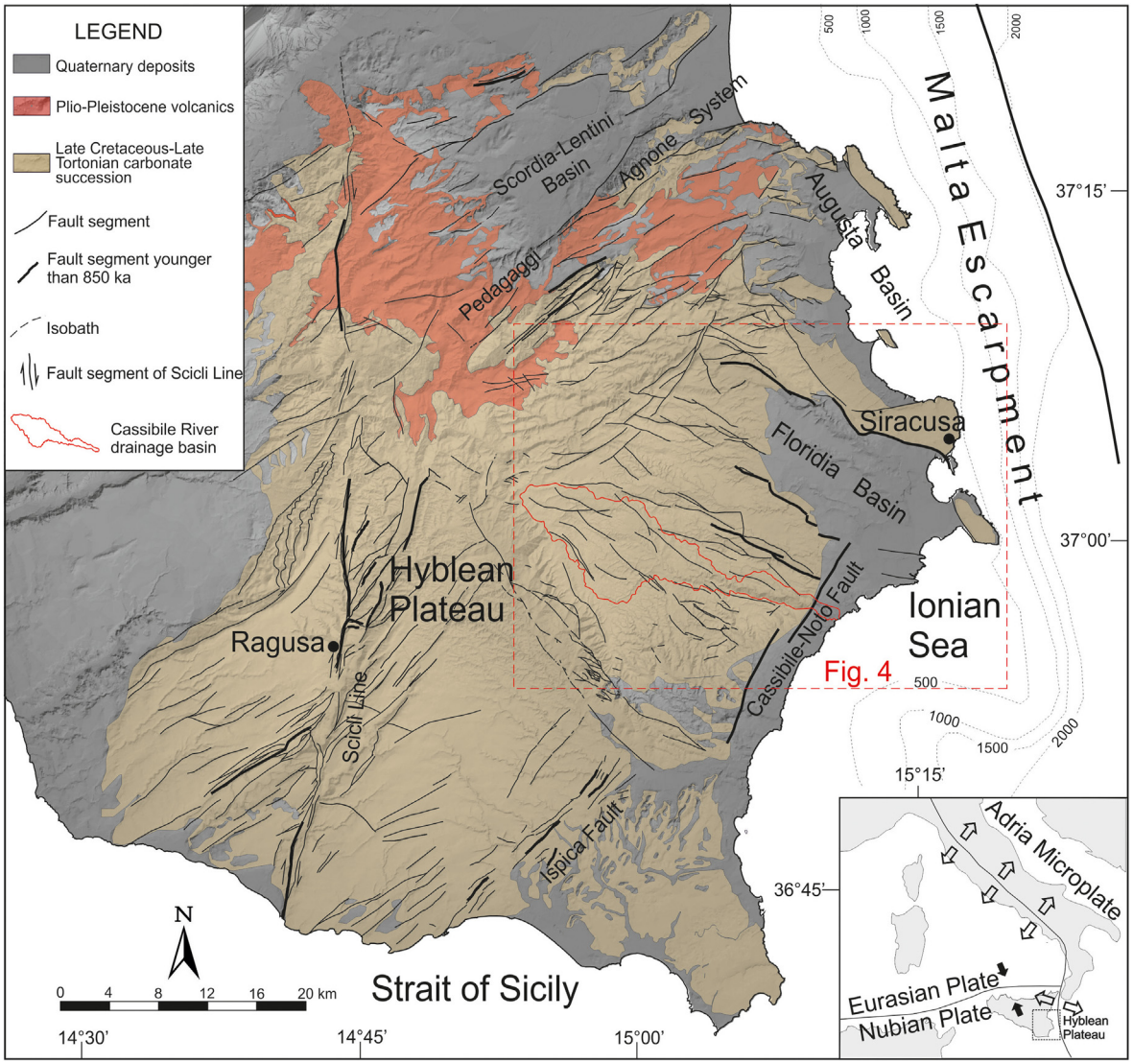

Fig. 1. Map showing the geological and structural setting of the Hyblean region (SE Sicily, Italy). The map also shows the drainage basin of the Cassibile River, analyzed in the present study.

and the eustatic highstands is the tool we use to date the paleo-river long profiles. This timing is validated by the compatibility of the resulting knickpoint travel times, namely the geomorphic response time to base-level falls, mostly depending on rock erodibility and climate.

We also document the wave-like migration (e.g., Loget and Van Den Driessche, 2009) of knickpoints and the related entrenching processes by exploring valley shape metrics (e.g. *Vf* distribution). By comparing the estimated incision rate with the uplift rate at the footwall of the Cassibile-Noto Fault, we validate the assumption of the steady state conditions of paleo-rivers, done to perform the river long profile analysis.

Finally, we propose a comprehensive time-space model for the fluvio-karst features, considering the combined effects of regional tectonic uplift and active fault-related deformation, via comparison of the age models obtained in the Floridia Basin and in the adjacent Cassibile River area, respectively.

2. Geological-structural and geomorphological setting

In the general geodynamic framework of the NNW-SSE oriented Nubia-Eurasia convergence (Serpelloni et al., 2007), the Hyblean Plateau in SE Sicily, represents an emerged sector of the African foreland domain (Burollet et al., 1978) separated from the Ionian Basin by the Malta Escarpment (Fig. 1). This comprises a Late Cretaceous-Late Tortonian carbonate succession comprising shallow water facies to the east, and deeper water basin facies to the west. During the Neogene, the ~30 km-thick African continental crust flexured under the load of the SE-verging allochthonous Sicilian thrust belt (Ben Avraham et al., 1990; Roure et al., 1990). Consequently, the Hyblean region was affected by extensional tectonics (Grasso and Reuther, 1988; Ben Avraham and Grasso, 1991). The northern sector of the plateau collapsed to form the NE-SW oriented Scordia-Lentini Basin (Ghisetti and Vezzani, 1980; Grasso and Reuther, 1988). To the west these extensional features are linked to the Scicli Line, a N10 degree trending, dextral fault zone (Catalano et al., 2008b) (Fig. 1). To the south, the tectonic boundary of the plateau is represented by two NE-SW oriented, SE-dipping normal faults, the Ispica and Cassibile-Noto faults (Catalano et al., 2008a; Pavano et al., 2019). In the general contractional framework of eastern Sicily (Monaco et al., 2002; Catalano et al., 2017), in the Middle Pleistocene (<850 ka), the tectonic configuration of the Hyblean region was reactivated by a deep-seated mantle intrusion (Catalano et al., 2010). The mantle upwelling resulted in positive tectonic inversion of the former extensional Neogene faults controlling the Scordia-Lentini Basin (Bousquet and Lanzafame, 2004; Catalano et al., 2010). Along the southern border of the Scordia-Lentini Basin (Pedagaggi-Agnone Fault system; see Fig. 1), NE-SW oriented, SE-dipping reverse faults were developed at a mesoscale across the previous N60 degree oriented, NW-dipping normal faults (Bousquet and Lanzafame, 2004). The remobilization by reverse motions along the northern border of the plateau produced a generalized SE-ward tilting of its eastern sector (Bonforte et al., 2015). Concurrently, in the western sector of the plateau, the Scicli Line was partially reactivated by sinistral motions (Catalano et al., 2008b, 2011), while extensional dynamics characterized the southeastern border of the plateau (Catalano et al., 2008a). Here, the extension was accommodated by the NNE-SSW-trending Cassibile-Noto and Ispica faults (Catalano et al., 2008a; Pavano et al., 2019). In addition, crustal stretching led to the development of the basin bounding NW-SE-oriented normal faults of the Floridia and Augusta Basins (Fig. 1).

The geological setting of the study area is almost uniform. The Floridia Basin is a tectonic depression infilled by Lower Pleistocene marly-clays passing laterally and upwards into calcarenites and sands. In the footwall of the border faults algal biolitites and calcarenites of the Monti Climiti Formation (Pedley, 1981; Carbone et al., 1987) extensively outcrop. To the south, most of the Cassibile River drainage basin is uniformly underlain by Miocene calcarenites and calcirudites of the Palazzolo Formation (Fig. 2). In the study area, the Palazzolo Formation is largely represented (~85%) by thick beds of white-yellowish crumbly calcarenites (Rigo and Barberi, 1959; Di Grande et al., 1982; Carbone et al., 1987). Almost 12% of the drainage basin is developed into alternating grey and marly limestone of the Palazzolo Formation, while only ~3% drains carbonates of the Monti Climiti Formation. At the drainage basin outlets, a very narrow coastal belt hosts Late Pleistocene marine terraces and alluvial fans (Pavano et al., 2019) fed by deeply incised canyons (Fig. 2).

The late Quaternary tectonic evolution of the Hyblean Plateau gave rise to its current geomorphological setting. The Hyblean Plateau is characterized by an elevated low-relief (~50 m) landscape (maximum elevation of ~980 m a.s.l.) (Fig. 3a) tilted to the SE (Bonforte et al., 2015). Some 90% of the drainage area of the Cassibile River lies between 350 m a.s.l. and ~700 m a.s.l. (Fig. 3b), with no local climate changes. The Cassibile River basin homogeneously receives an average annual rainfall of 650 mm (Osservatorio delle Acque, 2005; Regione Sicilia) (Fig. 3a), under fairly constant temperatures throughout the year (Liuzzo et al., 2017).

This summit landscape is deeply dissected by fluvial canyons (e.g., Cassibile River) which host a series of upstream migrating knickpoints along their main streams. These knickpoints have been generated by relative base-level falls linked to the long-term tectonic deformation of the Cassibile-Noto Fault (Pavano et al., 2019).

The Hyblean Plateau is bordered by several levels of marine terraces. These consist of wave-cut surfaces sometimes capped by thin sediment covers. The landwards inner edges represent the paleoshorelines that can be linked to the main interglacial Oxygen Isotope Stages (OISs) represented in the global eustatic curve (Chappel and Shackleton, 1986;

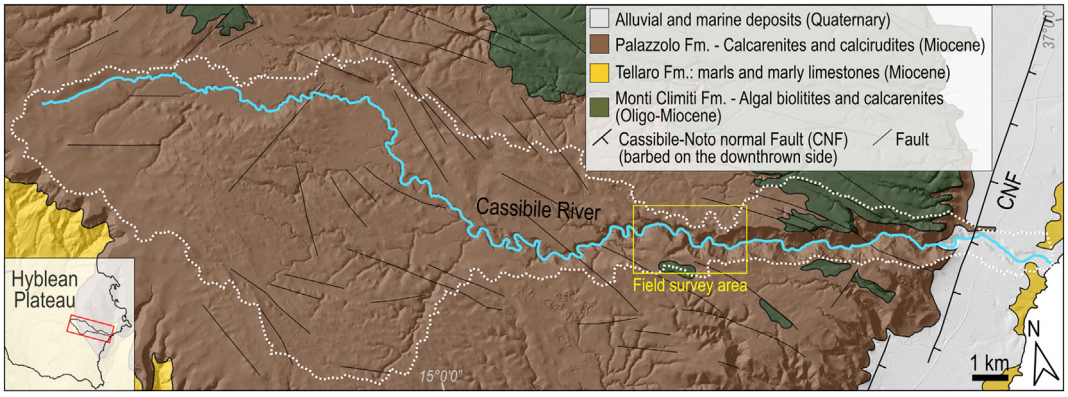

Fig. 2. Geological map of the Cassibile River basin area (see its location in the frame of the Hyblean Plateau in the inset map), showing the uniform distribution of lithologic units within the basin (modified from Lentini et al., 1984). CNF: Cassibile-Noto Fault (Pavano et al., 2019) (see the text for a detailed description of the geological units). The yellow box indicates the field survey location.

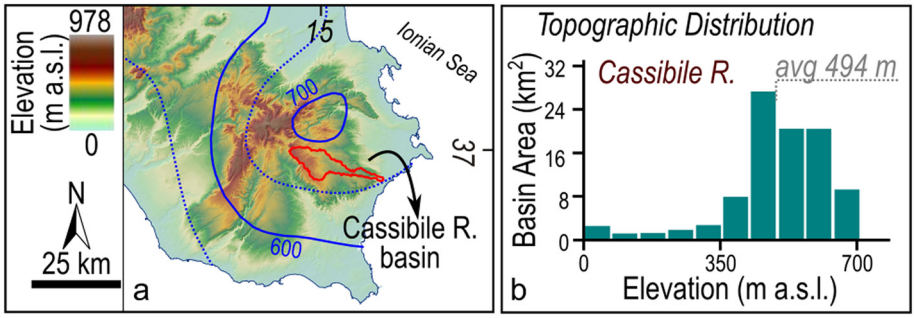

Fig. 3. a) Hillshade of the DEM of the Hyblean Plateau (see inset in Fig. 1 for location), showing the location of the Cassibile River basin. The blue numbered lines represent the contouring of the annual rainfall in mm/yr (source: Osservatorio delle Acque, 2005) (solid lines = 100 mm/yr, dotted lines = 50 mm/yr). Note that annually the Cassibile basin receives a uniform amount of rainfall of ~675 mm/yr; b) distribution of elevations through the Cassibile River basin, showing an average elevation of about 494 m a.s.l. (dotted grey line). Note that most of the basin area is at elevations higher than 350 m a.s.l.

Chappell et al., 1996; Waelbroeck et al., 2002; Siddall et al., 2003; Rohling et al., 2014).

Several age models have been proposed for the marine terraces and paleo-shorelines of the Hyblean Plateau (Antonioli et al., 2006; Ferranti et al., 2006; Catalano et al., 2008a; Dutton et al., 2009; Spampinato et al., 2011; Pavano et al., 2019). Although built by adopting different reference eustatic curves, the most complete works concerning the age attribution of the marine features of the study area have been provided by Bianca et al. (1999), Catalano et al. (2010) and Meschis et al. (2020). These models are based on radiometric and biostratigraphic dating of only a few terrace deposits.

The most spatially extended and complete age model has been proposed by Catalano et al., (2010), and is based on the analysis of 11 levels of marine terraces (Fig. 4). Two key dating approaches have enabled correlation of the flight of marine terraces to the main late Quaternary OISs of the Oxygen Isotope Timescale (Fig. A of supplementary material) (Bassinot et al., 1994). Firstly, Elephas falconeri teeth found in the infilling deposits of the Spinagallo karst cave (q in Fig. 4) were dated to 455 ± 90 ka using the isoleucine epimerization method (Bada et al., 1991; Bianca et al., 1999). The cave lies on a 125 m-high paleo-shoreline that has been attributed to OIS 13 (520 ka). Secondly, coarse-grained deposits overlapped by a marine terrace deposit contain 117 ka old mammal relics (Rhodes, 1996) and suggest an OIS 5.3 (100 ka) association. In addition, the uppermost marine terrace comprises an inner edge that has been assigned to the OIS 21 eustatic highstand (850 ka) (Catalano et al., 2008b), and is inset by the 520 kyr-old paleo-shoreline. Collectively, these marine terrace levels encompass a time span ranging from 850 ka to 570 ka. Consequently, an Early Pleistocene age (>850 ka) is inferred for the summit landscape of the plateau (Catalano et al., 2008b) (Fig. 4).

The onset of marine terracing has been associated with the early stages of tectonic uplift of the Hyblean region (Catalano et al., 2008a, 2010). The inferred long-term uplift-rates range from ~0.3 mm/yr in the Floridia Basin and Cassibile River area, to 0.7 mm/a, in the northern sector of the plateau (Fig. 1) (Catalano et al., 2010), thus confirming the southeastwards tilting of the region.

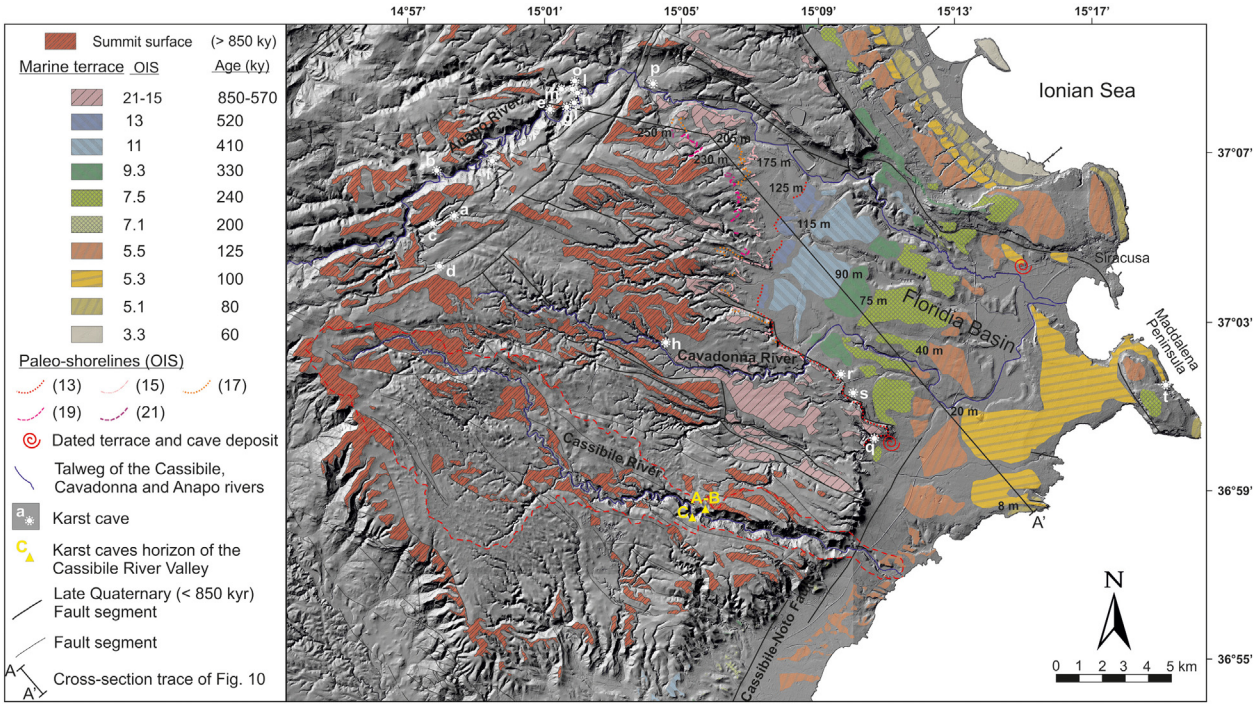

Fig. 4. Distribution of the Middle-Late Pleistocene marine terraces (data from Catalano et al., 2010) and paleo-shorelines (data modified from Di Grande and Raimondo, 1982) detected in the Floridia Basins and along the Cassibile-Noto Fault area (data from Pavano et al., 2019), draped on a high-resolution Digital Elevation Model (DEM). The location of the main karst caves (asterisks and triangles) documented in the region is also reported; the long-dashed red line represents the Cassibile River's drainage basin.

To the south, in the Cassibile River area, the ~300 m-high scarp of the Cassibile-Noto Fault hosts remnants of Late Pleistocene marine terraces (OISs 11-to-7) (Pavano et al., 2019). The younger marine terraces (OISs < 7) are widely preserved in the coastal plain (Bianca et al., 1999; Catalano et al., 2010; Pavano et al., 2019).

The Cassibile River watershed is dominated by a WNW-ESE-oriented canyon, which shows a narrow (2–3 km-wide) and deeply incised (up to 200–300 m) valley (Fig. 2). The most distinct geomorphic feature of the main channel of the Cassibile River is a 250 m-high and 7–8 km-long main knickpoint (Pavano et al., 2019). Along the entrenched portion of the valley, the deep incision has not preserved any fluvial terraces along the canyon, thus inhibiting any reconstruction of the paleo-streambed. Conversely, remnants of paleo-karst horizons are still preserved along the valley flanks, mainly represented by several cave entrances.

More generally, the carbonate sequences of the eastern sector of the Hyblean Plateau host a karst system arranged into different horizons. This system comprises both water-table and vadose epigenic caves (sensu Audra and Palmer, 2015) that have been documented by Ruggieri et al. (2007) for the Anapo River Valley, in the Floridia Basin (see location in Fig. 1). The authors recognized at least two main karst horizons located at elevation ranges of 210–260 m a.s.l. and 100–145 m a.s.l. These levels are considered to be associated with different stages of fluvio-karst stability, characterized by low rates of karst incision and by the infilling of conduits with continental sediments (e.g., "Grotta del Conglomerato"; l in Fig. 4). These two periods separate three stages of karst system deepening, represented by three arrays of karst morphologies distributed at elevation ranges of 260–550 m a.s.l., 145–210 m a.s.l. and <100 m a.s.l. (Ruggieri et al., 2007). Furthermore, Ruggieri et al. (2007), also attribute the cave system complexes characterized by different karst levels to a polyphase evolution associated with late Quaternary (<330 ka) marine transgression-regression episodes.

3. Methods

3.1. Cassibile River drainage basin

The analysis carried out in this study is focused on exploring the geomorphic features along the Cassibile River canyon (Hyblean Plateau) (Fig. 1) and their relationships with the karst forms developed along its valley walls. The uniform climate of the Cassibile River region (e.g., Osservatorio delle Acque, 2005; Liuzzo et al., 2017) rules out any major impact of local climatic variations on the geomorphic development. Additionally, we test if the locations of the knickpoints along the fluvial network of the Cassibile River have any dependency on the structural arrangement of the study area (Lentini et al., 1984). For this purpose, a density map of the fault segments mapped in the Cassibile River area has been created by using the Kernel density (Silverman, 1986) tool in ArcGIS 10.6 (search radius: 1 km) and compared with the k_{sn} map (Section 3.1.1).

Geomorphic analysis of the canyon has been supported by satellite image interpretation (e.g., Google Earth). Additionally, we carried out field surveys, aimed at documenting some specific karst morphologies configured into the canyon walls. Particular attention has been paid in the area surrounding the main knickpoint. Here, the uncertainty associated with the reconstructed paleo-profile is minimal, thus allowing correlation with the karst caves.

The morpho-tectonic evolutionary age model available for this sector of the eastern border of the Hyblean Plateau (Pavano et al., 2019) has been used as a space-time reference for the projection of the reconstructed river paleo-long profiles. Although the bedrock channel of the Cassibile River catchment (Fig. 1) is mostly underlain by carbonates (Rigo and Barberi, 1959), and although karst processes are active in the wider Hyblean region, the Cassibile River flows as a perennial river. Previous studies of river incision into karstified rocks (e.g., Anthony and Granger, 2007), has demonstrated that the stream power incision model can also be applied in such a geological setting. In cases where rivers experience a marked reduction of water discharge due to karst processes (Anthony and Granger, 2007), the values of the exponent of the channel slope of the stream power incision model (i.e. n) (Howard and Kerby, 1983) should be larger than 1. This is not the case for the Cassibile River, which shows no marked reduction in water discharge or disappearance of the stream into a karstic sub-surface.

3.1.1. Drainage system analysis

Along-stream fluvial geomorphic features (e.g., knickpoints) represent the most common geomorphic response of tectonic uplift pulses transiently shaping a stream's long profile. With uniform rock uplift, rock-type and climate setting, knickpoints represent mobile, time-dependent geomorphic markers. They migrate through a landscape at a rate inversely proportional to the drainage area (Wegmann and Pazzaglia, 2002; Kirby et al., 2003; Wobus et al., 2006; Pavano et al., 2016). The stream power incision model (Howard and Kerby, 1983) is most commonly used for describing the erosion (E) of a bedrock channel

$$E = K A^m S^n \tag{1}$$

where K ($m^{1-2m}\ yr^{-1}$) is the erosion coefficient linked to both climatic and lithological factors (Snyder et al., 2000), A (m^2) is the drainage area and S (dimensionless) is the channel slope. m and n are positive constants depending on the incision processes, hydrology and channel geometry (Whipple and Tucker, 1999; Whipple et al., 2000).

The model in Eq. (1) is usually expressed as a power law (Hack, 1957; Flint, 1974; Snyder et al., 2000; Kirby and Whipple, 2001) where the channel slope is positively correlated to the drainage area, a proxy for drainage discharge:

$$S = k_s \cdot A^{-\theta} \tag{2}$$

k_s ($m^{2\theta}$) represents the steepness index and θ is the dimensionless concavity index, that, in a logS-logA space, correspond to the y-intercept and the slope of the data regression line, respectively (Fig. 5a). θ was found varying between 0.3 and 0.6 (Whipple and Tucker, 1999; Snyder et al., 2000; Whipple, 2004; Wobus et al., 2006) and results from the ratio between m and n. This latter is reported to be ~1 (Whipple et al., 2000) for detachment-limited plucking erosion process (Hancock et al., 1998) in bedrock channels. A theoretical value of $\theta = 0.45$, is commonly applied as a reference (θref) to normalize the steepness index (k_{sn}) (Snyder et al., 2000; Kirby and Whipple, 2001; Wobus et al., 2006), as also used in the present study for the Cassibile River,

$$S = k_{sn} \cdot A^{-\theta ref} \tag{3}$$

Eq. (1) can be solved for local channel slope and rearranged into a similar form as per Eq. (2):

$$S = \left(\frac{E}{K}\right)^{\frac{1}{n}} A^{\frac{-m}{n}} \tag{4}$$

The comparison of Eqs. (1), (3) and (4), reveals k_{sn} ($m^{2\theta}$), when $n = 1$, is a function of erosion rate (E; mm/yr) and rock erodibility (K; $m^{1-2m}\ yr^{-1}$) (Kirby and Whipple, 2001; Snyder et al., 2000; Wobus et al., 2006). Assuming steady state conditions, where rock uplift (U) equals channel erosion (E) and $n = 1$ (Hancock et al., 1998), results in a simple relationship between k_{sn}, U and K:

$$k_{sn} = U/K \tag{5}$$

In the present study, k_s and θ values were extracted from the river long profile plotted in log$S$-log$A$ space (Fig. 5a). The purpose of the river long profile analysis is the reconstruction of the paleo-thalwegs downstream from a knickpoint (Fig. 5a). The trunk of the channel located upstream from a knickpoint is assumed to be the remnant of a previous steady paleo-river profile. Thus, knickpoint identification is

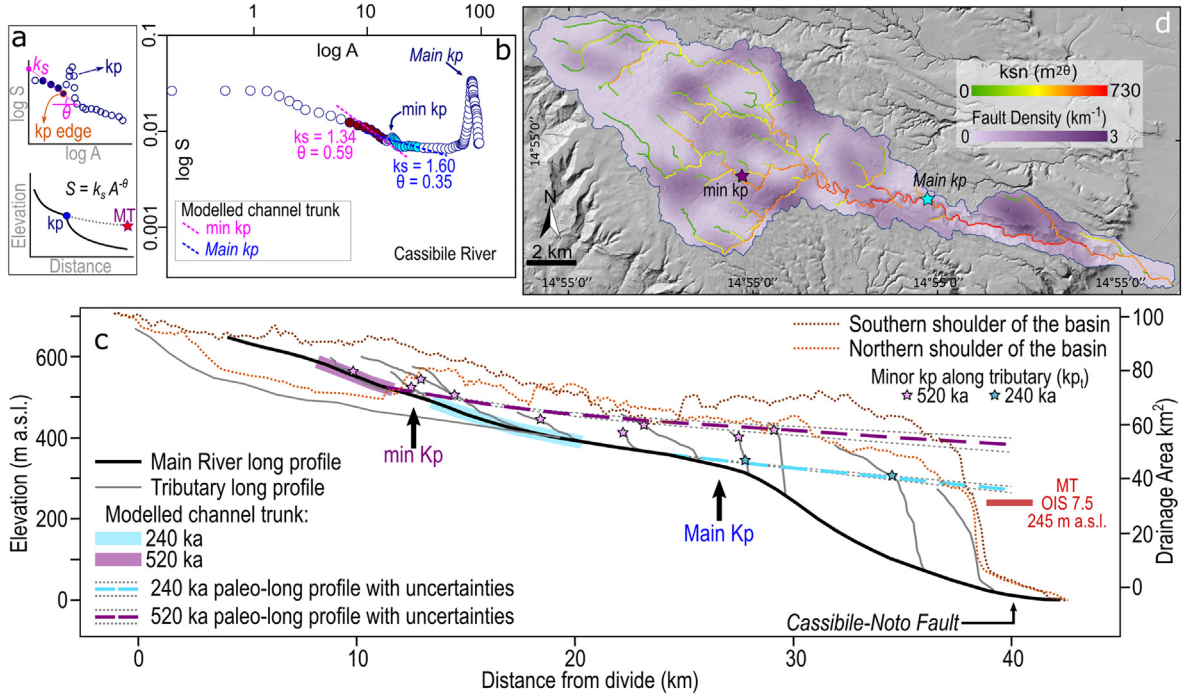

Fig. 5. a) Top: hypothetical logS-logA plot (blue circles) of a river profile with a migrating knickpoint (kp). The main elements considered for the identification of a knickpoint, its modelling and the paleo-long profile reconstruction are also reported; bottom: theoretical river long profile (black solid line) hosting a knickpoint (kp) and showing the reconstructed paleo-thalweg (dotted grey line), projected downstream to the location of remnants of marine terraces' strandlines (red star); MT: Marine Terrace. b) logS-logA space used to analyze river long profiles of the Cassibile River, modelling the channel trunks lying upstream of the identified knickpoints. The purple circles (linear regression: dashed pink line) refer to the modelled channel trunk upstream the minor knickpoint (min kp), whereas the light blue circles (linear regression: dashed blue line) refer to the modelled channel trunk upstream the main knickpoint (Main kp). The values of k_s and θ obtained for each trunk are also reported; c) Cassibile River's current and reconstructed long profiles with uncertainties (dotted light grey lines) plotted together with the long profiles of the main stream's tributaries. The location of the Cassibile-Noto Fault and the position of the remnants of marine terraces associated with the OIS 7.5 (Pavano et al., 2019) are also reported; d) map showing the distribution of the k_{sn} for the Cassibile River's fluvial network. In the background the distribution map of the fault line density is shown.

an important aspect of this analysis, and it has been determined accordingly from the logS-log*A* plot (Fig. 5a). In the same logS-logA space, we picked the k_s and θ values by regressing linearly the portion of the channel upstream from each knickpoint (Fig. 5a and b).

In this study, we reconstruct the profiles down to the Cassibile canyon's outlet (Fig. 5c), where several levels of marine terraces (OIS < 13) are developed into the scarp of the Cassibile-Noto normal fault (Pavano et al., 2019) (e.g., the marine terrace level associated with OIS 7.5). As well as the main channel profiles, we also plot the profiles of their minor tributaries. This allows us to identify minor knickpoints that could match the reconstructed paleo-thalweg. Thus, we can document the upstream propagation of the base-level-fall signal through the entire drainage network. In addition, given the uniform rock type, a k_{sn} ($\theta ref = 0.45$) distribution map, has been created to help locate knickpoints (Fig. 5d). To generate this map, we use the Matlab-based tools Topotoolbox (Schwanghart and Scherler, 2014, 2017).

The long profile analysis has been carried out by using a Digital Elevation Model (DEM) with a resolution of 2 × 2 m (derived and pre-elaborated from LiDAR data; ATA 2009 flight - Sicily Region). We chose such a detailed DEM for the high qualitative and quantitative landscape resolution provided. In fact, in deeply incised landscapes characterized by steep slopes, coarser resolution (e.g., 10–30 m) DEM products could have accuracy issues with the derived fluvial network and the river long profile analyses (e.g., Boulton and Stokes, 2018).

Using ArcGIS 10.6, we filled the DEM and extract the river long profile data using the Hydrology Tools. We apply a threshold reference for the drainage area of 0.5 km^2, which provides a resulting fluvial network that matches well the portion of the drainage system characterized by fluvial processes. We smooth the collected data within the SigmaPlot software using a 'loess' filter with a moving linear regression window one-tenth of the entire data set. Then, we analyze these data in Microsoft Excel, where we perform calculations for reconstructing the eroded portion of the long profiles located downstream from any knickpoint. Based on Flint's law in Eq. (2), these reconstructions are possible since we know the increments in river's distance (x) and in drainage area (A). Then, we obtain the channel slope (S) by using the extracted *ks* and θ. The distance and slope values allow us to calculate the elevation of the paleo-thalwegs that we reconstructed from the knickpoint edges down to the coast. The uncertainties related to these projections have been evaluated using a bootstrap sampling approach of the slope and area data of the modelled channel trunk located upstream from each knickpoint.

To determine the along-channel migration rate of the detected knickpoints, we applied a celerity model based on the stream power law of incision, according to Berlin and Anderson (2007). In this model, the knickpoint's retreat rate is a power function of the drainage area and erodibility (K) (with $n = 1$). We perform this evaluation according to the following steps. Firstly, we considered that throughout the study area the climate is uniform and assumed a constant drainage discharge. Thus, simplifying Eq. (1) and assuming $E = dz/dt$, the applied celerity model can be expressed by the following equation (Berlin and Anderson, 2007):

$$dx/dt = K \cdot A^m \tag{6}$$

where the ratio dx/dt is the migration rate of an upstream moving knickpoint. From Eq. (6), we derive the knickpoint's travel time (t)

$$t = \Sigma \left[dx_i / (K \cdot A_i^m) \right] \tag{7}$$

where dx_i represents along-channel discrete distance intervals, with constant length, and A_i is the corresponding drainage area at that

distance. This means that the argument of the summation in Eq. (7) represents the time that a knickpoint spends to cover an along-channel distance equal to dx_i. The travel time t is the time that the knickpoint spent to move from the valley's outlet to its current position, thus indicating the fluvial response time to a tectonic perturbation (Whipple and Tucker, 1999). This time span provides an approximation for the age of the paleo-long profile modelled before the base level dropped and that is still preserved upstream of the migrating knickpoint. To solve Eq. (7), we derived the value of the detachment-limited erosion coefficient (K) of 2.25×10^{-5} ($m^{1-2m}\,yr^{-1}$) from Eq. (5). We use the maximum uplift rate (~1.8 ± 0.05 mm/yr) estimated for the Cassibile-Noto Fault (Pavano et al., 2019) and the exponent of drainage area $m = 0.45$ ($n = 1$).

3.1.2. Valley shape analysis

An array of topographic sections transverse to the main axis of the canyon has been performed to obtain a geomorphological record (e.g., valley shape, width and depth) of the impact of the upstream, along-channel transit of the knickpoint. An equidistance of ~1 km between the sections has been chosen taking into consideration the occurrence of different geomorphic features along the valley (e.g., landslides, meanders, sinuosity, tributaries confluences). The length of the section corresponds to the distance, side by side, between the two opposite margins of the canyon and consists of twins of points located at the topographic cutoff that separates the almost flat summit surface of the plateau and the steep valley walls. To quantitatively trace the upstream propagation of knickpoint transit, and to document its ongoing migration, we also calculate the *Vf* index (Bull and McFadden, 1977; Bull, 1978). This index allows us to map the current location of i) the steady, ii) the already adjusted and iii) the rejuvenating sectors of the main valley across the knickpoint. The *Vf* index is represented by the ratio between the valley floor width and the average valley height

$$Vf = 2V_{fw}/(H_{ld} + H_{rd} - 2H_{SC}) \quad (8)$$

where V_{fw} is the valley floor width, H_{ld} and H_{rd} are the elevations of the left and right sides of the valley, respectively, whereas H_{SC} is the averaged elevation of the valley floor. $Vf \leq 1$ are associated to V-shaped valleys due to entrenched channels, whereas $Vf > 1$ corresponds to drainage system steadiness and fluvial aggradation (Keller, 1986; Keller and Pinter, 2002).

3.2. Floridia basin: marine terrace and karst cave correlation

Many studies have shown that speleogenesis and surficial geomorphological processes are connected (e.g., Palmer, 1987; Stock et al., 2005; Despain and Stock, 2005; Springer et al., 2015). Their relationships are influenced by many factors, such as eustatic variations, climatic changes, tectonic motions (uplift and subsidence) and fluvial dynamics (e.g. knickpoint retreat, fluvial discharge and/or sediment load, etc.) (Ambert and Ambert, 1995; Audra et al., 2001; Harmand et al., 2004; Wang et al., 2004; Mocochain et al., 2009; Guifang et al., 2011; Ortega et al., 2013; Tassy et al., 2013). For the Floridia Basin area, we distinguish two sectors, characterized by different types of karst cave arrangement: the coastal sector and the hill sector. Along the coastal plain (up to 150 m a.s.l.), water-table caves have formed near to the paleo-sea level and/or carved along a paleo-shoreline (Ruggieri et al., 2007). Thus, the analyzed karst features are considered as the product of dissolution near the base level. For this reason, for the coastal sector of the Floridia Basin, we followed the approach that Florea and Vacher (2006) and Canora et al. (2012) applied in Florida (USA) and in Apulia (southern Italy), respectively. These authors correlate the mapped paleo-karst caves with the marine terrace levels and their paleo-shorelines located at similar elevations. For the Floridia Basin area, although different marine terrace age models are available, we used the model proposed by Catalano et al. (2010). Firstly, this is because the model defines a tectonic setting responsible for the deformation of the onshore Hyblean region supported by field-based structural geological evidence. Secondly, the model proposes uplift-rates that are in good agreement with other studies (Bianca et al., 1999; Scicchitano et al., 2008; Spampinato et al., 2011).

Conversely, in the case of the hill sector, where the karst caves are located along the steep flanks of entrenched valleys, we follow the *per descensum* evolutionary model of karst systems (Palmer, 1987; Audra et al., 2001; Abel et al., 2002; Harmand et al., 2017), proposed for regions like the Hyblean Plateau. This model considers the speleogenesis to be related to the subsequent lowering of base level (local or global). In this context, the inland water-table consistently deepens. The model also considers that the horizontal development of a karst level occurs during stages of relative base level stability. The evolution of the karst system is governed by eustatic variation of sea level. Flooding and filling of karst caves and conduits occur during base level highstands. Coupled with water-table lowering is the entrenchment of the fluvial network that erodes towards the new lowered base level. As for the inland Hyblean region, the lowering of the karst system was coupled along the coastal area by the formation of paleo-shorelines and marine terraces. These processes are sustained by persistent, regional tectonic uplift and modulated by climatically forced eustatic oscillations (Fig. 6a–c).

By applying this model, we dated the karst caves of the Floridia Basin described by Ruggieri et al. (2007). We associate the karst caves to phases of rising sea level, testified by the marine terraces dated by Catalano et al. (2010). We chose the Floridia Basin region because of the absence, unlike the Cassibile River area, of a tectonic disturbance in the lateral continuity between the karst horizons and the dated marine terraces and paleo-shorelines along the coast. Data regarding these caves (e.g., location, elevation, etc.) are available in the catalogue of the caves located in the Siracusa territory (Piano Paesaggistico Ambiti 14–17 Siracusa - Schede Geotopi of the Regione Siciliana, 2018; https://www2.regione.sicilia.it/beniculturali/dirbenicult/bca/ptpr/documentazione_siracusa/ALLEGATI/schede_geotopi%20SR.pdf).

4. Results

From the geomorphic analysis of the Cassibile River's long profile we recognized and analyzed two knickpoints (Fig. 5b–c), a prominent one (main knickpoint – topographic relief in the order of 10^2 m) downstream, and a minor knickpoint (relief in the order of 10^1 m) located upstream in the upper portion of the basin.

The main knickpoint is located at about 15 km upstream from the coastline, at an elevation of about 380 m a.s.l. (Fig. 5c). The main drop in elevation across the knickpoint occurs relatively close to the coast within a distance of <10 km where the major Cassibile-Noto Fault is located. The position of this knickpoint is also well documented by the distribution of k_{sn} values (Fig. 5d). This metric shows its highest values, up to ~750 $m^{2\theta}$, in correspondence with the knickpoint, dropping downstream to values of <250 $m^{2\theta}$. Lower k_{sn} values of <50 $m^{2\theta}$ are widespread, extensively characterizing the entire upstream sector of the fluvial network (Fig. 5d). The geomorphic analysis also reveals a spatial mismatch between the k_{sn} metric and the distribution of fault segment density (Fig. 5d). The intensely fractured sectors of the Cassibile River basin, potential sites of fault-related rock weakening or fault scarps, not necessarily show spikes in k_{sn} along the adjacent fluvial network.

The channel's relict reach, located upstream from the main knickpoint, projects downstream close to the location of the hanging fluvio-karst morphologies (e.g., caves in Fig. 7). Along the coast, the reconstructed paleo-thalweg intercepts the Cassibile-Noto fault scarp at an elevation of ~260 ± 10 m a.s.l. Along the fault scarp, remnants of the OIS 7.5 (240 ka) marine terrace occurs at an elevation of ~245 m a.s.l. (Pavano et al., 2019) (Fig. 5c). The applied celerity model provides a travel time for this knickpoint of ~210 ± 7 kyr.

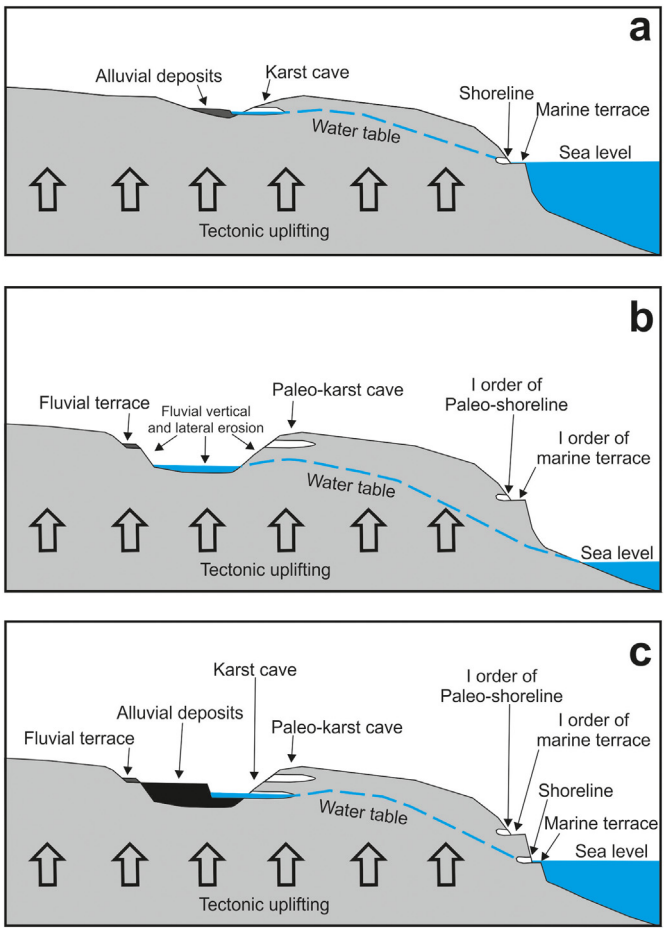

Fig. 6. Conceptual model of river entrenchment with formation of different karst levels during the earliest phases of the late Quaternary tectonic uplifting of the Floridia Basin area; a) during a first interglacial phase, the forming caves are located originally at the position of the paleo-valley's bottom. At the same time, a shoreline develops at the sea-level along the coast; b) during the subsequent cooling phase, combined with persistent tectonic uplift, the fluvial vertical entrenchment and lateral erosion produce a separation between the relict caves and the active valley's bottom, while the former shoreline is abandoned; c) during a second interglacial phase new karst caves develop at the river's bottom, while the older caves rests hanging on the valley's flank. In the coastal area, a younger shoreline is modelled at the new sea-level, while the older paleo-shoreline is preserved at higher elevation along the sea cliff.

Furthermore, using the minor knickpoint recorded at ~500 m a.s.l., some ~30 km from the coastline, we reconstructed a paleo-thalweg projecting downstream to a higher elevation of ~375 ± 17 m a.s.l. (Fig. 5c). The applied celerity model provides an estimate of this minor knickpoint's travel time of ~482 ± 16 kyr. For both reconstructed paleo-thalwegs, the long profiles of most of the Cassibile River's tributaries show minor knickpoints (kp_t in Fig. 5c).

The entire sector of the Cassibile River valley coincident with the main knickpoint (Fig. 8a) is deeply entrenched (Fig. 8b and c), with a maximum local relief of ~330 m (Fig. 8d). In addition, while the drainage basin narrows downstream, the entrenched canyon becomes wider downstream. In particular, the sector of the canyon hosting the main knickpoint is wider and more deeply entrenched than that located upstream. Similar results are derived from the along-channel distribution of *Vf* (associated uniform uncertainty of 0.01) (Fig. 8c). Along the valley, although *Vf* tends to be below 1, relatively higher values of up to ~0.35 ± 0.01, characterize the channel trunk upstream from the main knickpoint. Conversely, the lower portion of the canyon, located downstream from the main knickpoint, shows very low values in *Vf*, up to and close to 0 near the location of the caves (Fig. 8c). Further downstream, close to the valley outlet, *Vf* increases again, reaching values of ~0.25 ± 0.01 and ~0.4 ± 0.01.

Moreover, near the valley mouth and where the maximum topographic relief (*TR*) has been measured (Fig. 8d), the entrenched Cassibile River canyon shows a width of ~1 km, reducing to ~0.7–0.5 km in the proximity of the knickpoint and finally passing to lower values of up to ~0.15 km width in the upstream trunk of the valley. Proceeding further upstream, the topographic relief passes from ~330 m, near the canyon outlet, to ~250 m in the knickpoint sector, with values of up to <100 m in the upland region (Fig. 8d).

The field survey carried out along the central sector of the Cassibile River valley (Fig. 2), close to the current position of the main knickpoint, enables the identification of an array of karst caves. These features represent a karst horizon consisting of two main caves (Caves A and B, proceeding upstream) with entrances visible along the northern walls of the canyon (Figs. 4, 7a–b and 9). They are located near the knickpoint's edge, at elevations of ~340–350 m a.s.l. (Figs. 4 and 7a), ~20–30 m above the modelled paleo-thalweg associated with the OIS 7.5 (240 ka). In particular, the horizon along which the caves are positioned slopes slightly towards the east and does not parallel the nearly horizontal carbonate stratigraphic layering (Fig. 9). About 1 km upstream from these caves, in the opposite canyon wall, an additional karst cave (Cave C in Fig. 7a), widely exploited as rupestrian housing system (Nastasi et al., 2014), occurs. The lowest layer of this multi-level complex occurs at an elevation of ~365 m a.s.l., consistent with the karst horizon of Caves A and B.

To the north, in the Floridia Basin, where a complete flight of marine terraces occurs without any fault disturbance (Fig. 4), we tentatively developed an age model for the mapped karst features using the methodologies outlined in Section 3.

Most of the considered caves (e.g. the San Micidiario, Scale, Massi, Conglomerato, Tunnel and Pipistrelli caves; e, g, i, l, m, n, o in Fig. 4

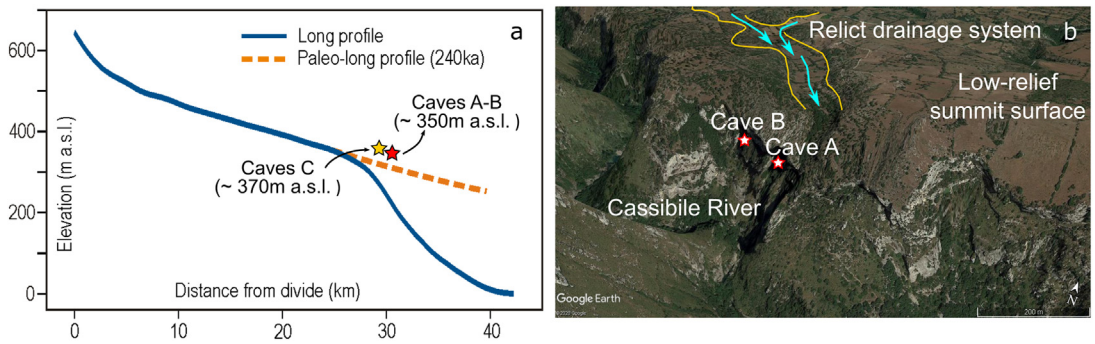

Fig. 7. a) Location of the detected karst morphologies (caves A and B, red star, and Cave C, yellow star) plotted against the long profile reconstructed from the main knickpoint detected along the Cassibile River; b) location of the karst morphologies (caves A and B) plotted in (a) along the left wall of the Cassibile River valley (source: Google Earth). The relicts of a paleo-drainage system imprinted into the summit low-relief landscape and the paleo-flow direction are also reported.

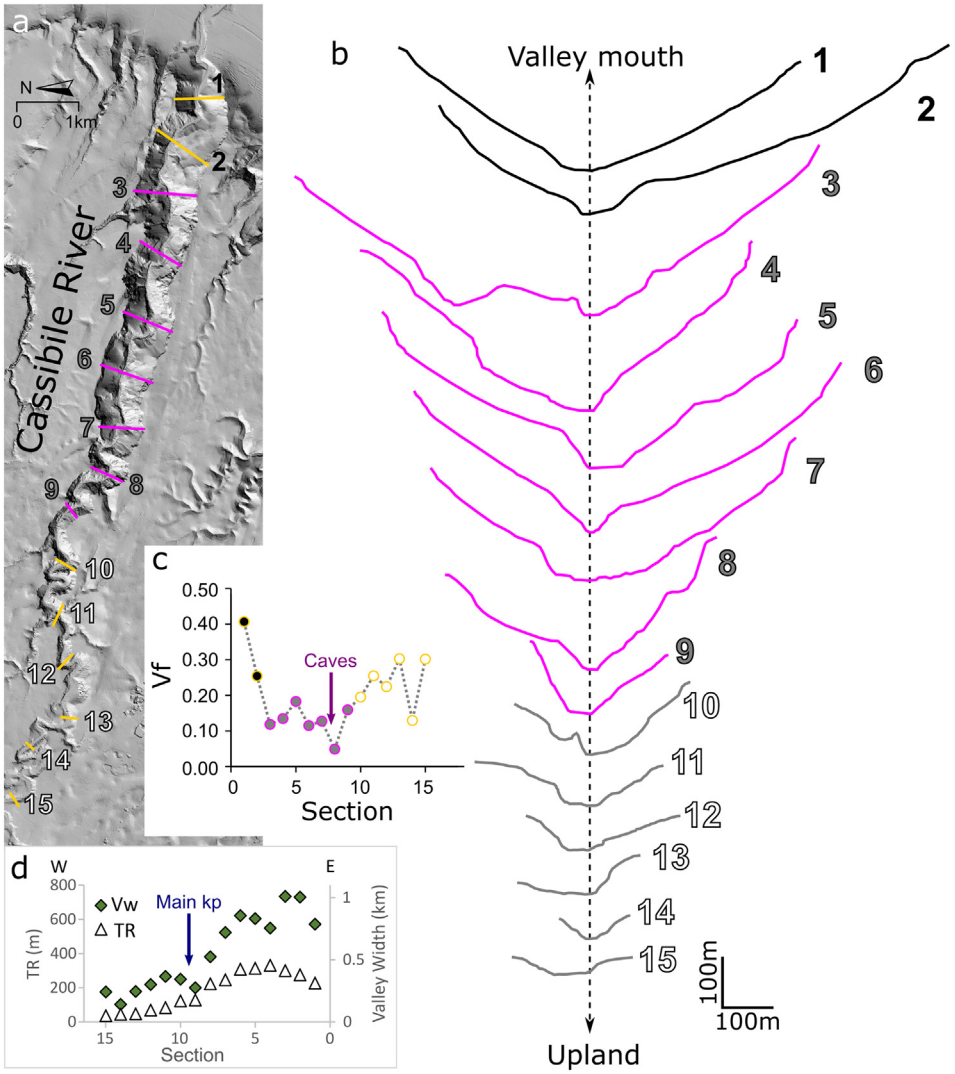

Fig. 8. a) Distribution of the topographic sections, spaced about 1 km from each other, transversally to the Cassibile River valley; b) topographic sections stacked top to bottom from the valley outlet to the upstream sector. The different colors refer to the different sectors of the valley: black refers to the sector of the valley downstream from the main knickpoint, pink to the main knickpoint interference zone and light grey to the channel trunk upstream the main knickpoint; c) distribution through the valley of the *Vf* values. The different colors of the circles' edges correspond to those of the section in a. The location of caves is also reported; d) along-valley variation of topographic relief (*TR*) (triangles) and valley width (V_W) (diamonds). The position of the main knickpoint is also indicated in the plot. Note that in c) and d) the associated uncertainties are too small (*Vf* = ±0.01; Vw and *TR* = ±4 m) to be clearly visualized in the plot.

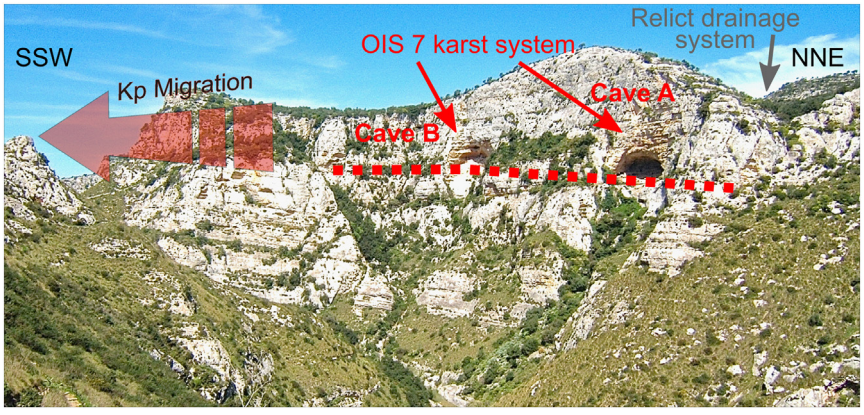

Fig. 9. Picture showing the relationships between the upstream migrating knickpoint along the Cassibile River canyon and the paleo-water-table associated with the OIS 7 (200–240 ka), which emerges at about 350 m a.s.l. as hanging karst caves (Cave A and Cave B) along the northern flank of the valley. Relict drainage system is also indicated in the picture.

and Table 1, respectively) are developed at elevations ranging from 530 m a.s.l. to 210 m a.s.l., along the highest sector of the Anapo River valley. Using the available models of karst level evolution in entrenching rivers of tectonically uplifted plateaus (Audra et al., 2001; Abel et al., 2002; Harmand et al., 2017) (Fig. 6) these karst caves are likely to have been associated with a succession of glacial-interglacial cycles and/or sub-cycles. In the absence of absolute dating, we cannot assign these highest caves to specific OISs. Thus, we tentatively correlate them across a range of OISs occurring in age between 850 ka (OIS 21), which marks the beginning of the tectonic uplift of the region (Catalano et al., 2008a, 2010), and 570 ka (OIS 15) (Fig. 4 and Table 1), when the marine terracing along the coastal plain commenced (Catalano et al., 2010). During this time span, the highest paleo-shorelines recognized in the Floridia Basin, which have been assigned to the main interglacial peaks of the eustatic curve, developed between 5 and 8 km distance from these caves. A more convincing correlation is between the "Grotta del Covo" (cave h in Fig. 4 and Table 1), at the outer-edge of the summit low relief surface of the Hyblean Plateau, and the adjacent inner-edge of the upper marine platform assigned to 850 kyr.

The other karst caves included in Table 1 develop at lower elevations in the Floridia Basin coastal plain. These caves are located at elevations consistent with those of the marine terraces and paleo-shorelines mapped by Catalano et al. (2010) (see Section 3), thus allowing their direct correlation. The "Grotta Spinagallo" (cave q in Fig. 4 and Table 1) has already been correlated by Catalano et al. (2010) to the 125 m-high paleo-shoreline, assigned to OIS 13 (520 ka) (see Section 2 for details). To the north, the "Grotta Chiusazza" and "Grotta Monello" (caves r and s in Fig. 4 and Table 1, respectively), located at about 100 m a.s.l., can be correlated with the marine platform lying at 90 m a.s.l. (Table 1), assigned to OIS 9.3 (330 ka; Catalano et al., 2010).

Further to the east, in the Maddalena Peninsula, the "Grotta del Pellegrino" (cave t in Fig. 4 and Table 1) is developed at an elevation of 10 m, on the notch level associated with OIS 5.1 (80 ka).

5. Discussion

In this study, we constrained an age model of karst features, combining their morphological relationships with both marine terraces and reconstructed river long profiles. We test a new approach that considers the cumulative effects of active deformation through time. Strandlines of a flight of marine terraces provide continuous space-time reference lines that are geographically restricted to the coastal area. In contrast, river long profiles form space-time reference lines that extend inland, connecting the related karst caves system to the correlative marine paleo-shorelines. In tectonically active regions, these reference lines progressively deform. They represent an important tool for the visualization and the partitioning in time of the cumulative effects of the tectonic processes. They thus provide the necessary constraints for lateral correlation of deformed landforms.

We tested our approach on the spatially extensive Hyblean carbonate region in southeastern Sicily, that experienced a Middle-Late Pleistocene (<850 ka) tectonic uplift (Catalano et al., 2010; Bonforte et al., 2015). This uplift is documented by marine terracing along the coastal slope, and by deep river entrenchment inland. The Floridia Basin was subjected to almost spatially uniform uplift related to a regional tectonic signal that, interacting with the eustatic changes, produced wide flat marine terraces. In the adjacent area of the Cassibile River valley, the marine strandlines are strongly deformed giving rise to an antiform fold geometry. This antiform marks the footwall of the NE-trending Cassibile-Noto normal fault. Strandlines culminate at the Cassibile River and converge towards the northern tip of the fault in the direction of the Floridia Basin (Pavano et al., 2019).

The age model of marine terraces (Catalano et al., 2010) and a reliable altimetric correlation of the karst features with the elevation of the continuous marine strandlines (Florea and Vacher, 2006; Canora et al., 2012), was firstly obtained in the Floridia Basin. For the correlation, we considered the *per descensum* evolutionary model of karst systems (Audra et al., 2001; Abel et al., 2002; Harmand et al., 2017), linking the deepening of the karst network to the base-level fall and river entrenchment. The karst cave levels mapped in the Floridia Basin lie below the oldest summit surface dated back to age > 850 ka (Catalano et al., 2010; Bonforte et al., 2015) (Fig. 10). The uppermost levels, exposed along the northwestern margin of the basin (i.e., upper Anapo River valley), pre-dates the 520 ka (OIS 13) marine strandline. The lowermost levels, exposed within the flight of marine terraces, correlate with marine strandlines ranging in age from 520 ka (OIS 13) and 80 ka (OIS 5.1) (Fig. 10 and Table 1).

The altimetric correlation, as performed for the Floridia Basin, does not apply to the tectonically-controlled Cassibile River area. The local

Table 1
Distribution of the karst caves, paleo-shorelines and marine terraces mapped in the eastern sector of the Hyblean Plateau. The karst caves from a to p have been correlated to the paleo-shorelines ranging in age between 850 ka (OIS 21) and 570 ka (OIS 15), whereas the caves from q to t have been assigned to single paleo-shorelines and/or marine terraces <520 ka in age (<OIS 13). The location of the caves (coordinates GAUSS-BOAGA expressed in meters) are from the "Piano Paesaggistico Ambiti 14-17 Siracusa - Schede Geotopi of the Regione Siciliana" (https://www2.regione.sicilia.it/beniculturali/dirbenicult/bca/ptpr/documentazione_siracusa/ALLEGATI/schede_geotopi%20SR.pdf). The corresponding OIS and modelled age (ka) are also reported.

Karst caves (m a.s.l.)	Name	Latitude	Longitude	Paleoshorelines (m a.s.l.)	Marine terraces (m a.s.l.)	OIS	Age (ka)
a (530)	Signore 2	4104893	2517368		–		
b (525)	Anapo 2	4106895	2516726	250			
c (500)	Signore 1	4104585	2516504				
d (425)	Anapo 1	4102644	2516783			21	850
e (375)	San Micidiario	4109408	2521674				
f (350)	Anapo 4	4107235	2519047	230			
g (305)	Scale	4109592	2522444				
h (300)	Covo	4099348	2526359			19	770
i (295)	Massi	4109717	2522694				
l (280)	Conglomerato	4110460	2522773	205			
m (260)	Tunnel	4110532	2522650		–		
n (250)	Trovata	4110300	2522930		–	17	690
o (225)	Pipistrelli	4110683	2522715	175	–		
p (210)	Vignale	4110596	2526252		–		
						15	570
q (125)	Spinagallo	4095263	2536149	125	125	13	520
r (110)	Chiusazza	4097786	2534193	90	90	9.3	330
s (105)	Monello	4096863	2534738	90	90	9.3	330
t (10)	Pellegrino	4097452	2548376	10	10	5.1	80

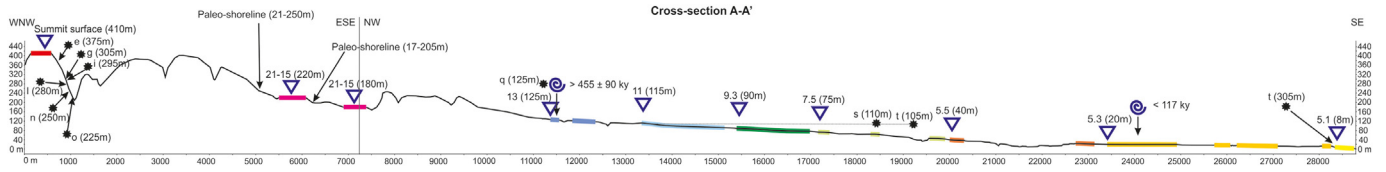

Fig. 10. Topographic section showing the entire flight of marine terraces within the Floridia Basin. The location and elevation of the marine terraces' inner-edges (labelled upside-down triangles), the location of the dated terraces (labelled spirals) and the projection of the karst caves (asterisks) and their elevations (m a.s.l.) are also reported.

contribution of the footwall uplift along the Cassibile-Noto normal fault caused lateral variability in the elevation of morphological features of the same age (Fig. 11a). In this circumstance, the reconstruction of paleo-long profiles of the river network provided isochronal lines bridging the coeval marine features cut into the fault scarp and the inland fluvial paleo-landforms (Crosby and Whipple, 2006; Kirby and Whipple, 2012; Gallen et al., 2013; Pavano et al., 2016; Jaiswara et al., 2019) (Fig. 11b). Inland, as suggested by the mismatch between k_{sn} map and faults density, the detected knickpoints cannot be associated neither with the location of secondary fault scarps nor with fault-related rock erodibility changes (rock weakening). We based the age model of our reconstructed paleo-long-profiles on the matching of their downstream projection to the Cassibile-Noto Fault scarp with the elevation of the marine strandlines (Fig. 5c). We validate the age model applying the celerity model of knickpoint migration responsible for the progressive entrenchment of the analyzed long profiles. The reconstructed paleo-long profiles and the resulting ages suggest that the paleo-thalwegs were formed between 520 ka and 200–240 ka. The lower paleo-long profile, reconstructed from the main knickpoint, can be associated with the OIS 7 (200–240 ka) highstand. In fact, its downstream projection to ~260 ± 10 m a.s.l. matches the elevation of the corresponding marine terraces' strandlines, currently preserved along the Cassibile-Noto Fault scarp at an elevation of 245 m a.s.l. The paleo-thalweg that was reconstructed by modelling the trunk channel above the minor knickpoint projects downstream to an elevation of ~375 ± 17 m a.s.l., and it has been associated with OIS 13 (520 ka) (Fig. 5c). This projected elevation is compatible with the alignment of the tributary confluences. These confluences are now truncated and abandoned on the summit of the low-relief landscape of the Hyblean Plateau at the rim of the canyon (Figs. 7b and 9). Furthermore, the tributary channel long profiles show knickpoints that approach the position of both the paleo-thalwegs, reconstructed using both the main and minor knickpoints. These tributary channel knickpoints are also evident in the k_{sn} distribution (Fig. 5d). Locally, these tributary knickpoints show a recessed position with respect to the location of the main channel confluence. This would suggest that the erosion related to knickpoint migrations along the main channel of the Cassibile River is propagating upstream along the entire fluvial network (Fig. 5c). In the context of the tectonic deformation model of the eastern Hyblean Plateau, the paleo-long profile reconstructed from the minor knickpoint could be associated with an early stage of river incision. This is similar to that reconstructed for the upper sector of the Anapo River Valley in the Floridia Basin (Fig. 11c). Furthermore, this paleo-long profile was entrenched as a consequence of the early (<850 ka; Catalano et al., 2010) stages of uplift experienced by the eastern Hyblean Plateau's crustal block (Catalano et al., 2010). This would imply that most of the local relief along the upstream portion of the Cassibile River (Fig. 7d) (i.e. accumulated between the top of the plateau summit surface and the 520 ka paleo-long profile) was likely developed between 850 ka (Catalano et al., 2010) and 520 ka (OIS 13).

By combining the two reconstructed paleo-long profiles, the maximum discrepancy in elevation between the two is ~100 m. This would result from a channel lowering stage that occurred between 520 ka and 200–240 ka. Thus, given the 280–320 kyr time span, the resulting incision rate is ~0.31–0.35 mm/yr. This value approaches the 0.3 mm/yr regional long-term uplift rate reconstructed for this sector of the Hyblean region during the last 850 kyr (Catalano et al., 2010; Bonforte et al., 2015). First of all, these results validate the assumption we did for the river long profile analysis about the steady state conditions for the paleo-rivers at the footwall of the Cassibile-Noto Fault. These data suggest that the Middle-Late Pleistocene uplift rate was balanced by the long-term incision rate prior to the occurrence of the main base level drop at about 200–240 ka. This base-level lowering subsequently

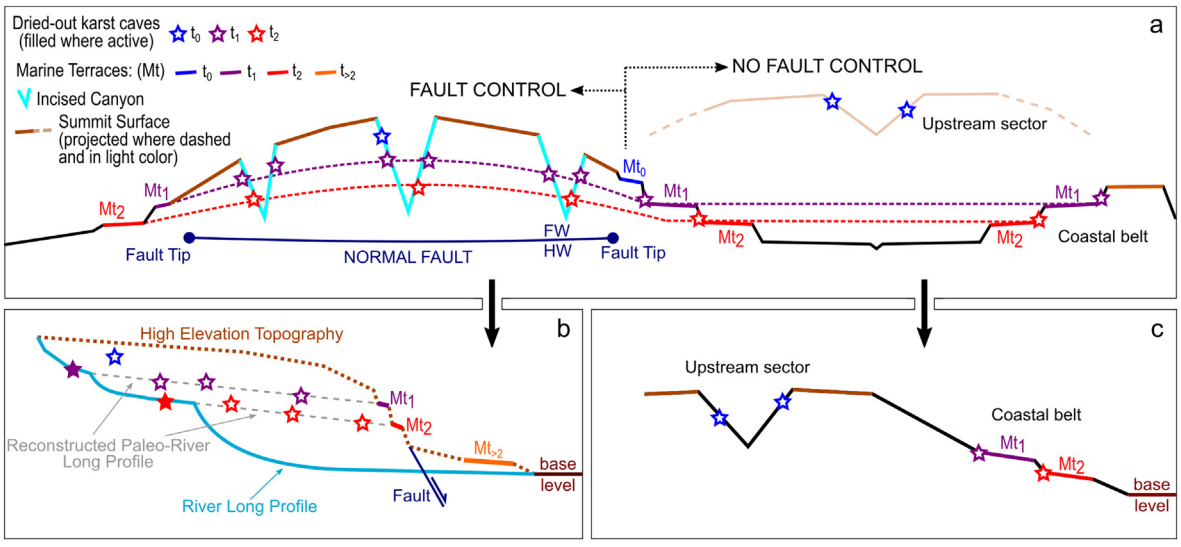

Fig. 11. a) Schematic section across the study area, from the fault-controlled (normal fault) sector of the Cassibile River, to the Floridia Basin, which uniformly recorded the regional component of uplift. FW: Footwall; HW: Hanging Wall; b) schematic river long profile showing the relationships between knickpoints, reconstructed paleo-river long profiles and exhumed karst horizons, in the context of a fault-controlled landscape setting (Cassibile R.); c) schematic section across the Floridia Basin, showing the relationship between the upstream sector and the lowland one, in the context of a uniformly elevated landscape according to the regional component of uplift.

caused the deep entrenchment of the canyon and the development of the main knickpoint. The geomorphic analysis highlights that, since the Late Pleistocene, the Cassibile River valley is still experiencing channel lowering and canyon widening, due to the upstream transit of the main knickpoint (Fig. 7). This is corroborated by both the along-valley changes in *Vf* index, close to 0 in the canyon-like sector of the valley, and by the spatial distribution of the topographic relief and canyon width. Indeed, these metrics markedly decrease upstream, proceeding from the canyon outlet to the upland region of the Hyblean Plateau (Fig. 7). This change in valley width in response to fault-related increase in uplift rate has also been documented for other areas, including the Mediterranean region (e.g., Whittaker et al., 2007, 2008). Our data indicate that early channel entrenchment, due to tectonic uplift, and the resulting channel narrowing are processes that migrate upstream coupled with the moving knickpoint. This leaves space downstream for the channel to reduce its slope angle (Whittaker et al., 2008), adjusted to a constant (steady) uplift rate.

Moreover, the base-level lowering caused the deepening of the water-table and the incision of the paleo-riverbed by the migration of the knickpoint towards the upstream sectors of the Cassibile River catchment (Fig. 9). Consequently, during the upstream-migrating wave of fluvial erosion, the abandoned paleo-karst system, which is believed developed around the paleo-water-table related to the corresponding eustatic highstand, was exhumed. Thus, Caves A-C would represent evidence for an exhumed paleo-water-table position developed during OIS 7 (240 ka) in the Cassibile River area (Fig. 9).

Finally, by applying the celerity model we also estimated the cave exhumation age due to the transit of the main knickpoint. This age corresponds to the travel time needed for incision to migrate from the Cassibile-Noto Fault up to the location of karst cave complex. The karst morphologies recorded along the northern wall of the Cassibile River canyon are located at ~9 km from the Cassibile-Noto Fault and the celerity model suggests that the caves were exhumed ~110 kyr ago. This infers a knickpoint migration rate of ~82 ± 3 m ky^{-1}. This value is in good agreement and in the same order of rates (10^1–10^2 m ky^{-1}) proposed in previous published data collected globally, including the Mediterranean area (e.g., Hayakawa and Matsukura, 2003; Bishop et al., 2005; Anthony and Granger, 2007; Whittaker and Boulton, 2012). It also well fits the average distribution of knickpoint migration rate for bedrock channels as a function of the drainage area (e.g., Loget and Van Den Driessche, 2009).

6. Conclusions

In this study we apply an age model to karst systems using reconstructed space-time reference lines, including paleo-river long profiles and marine strandlines. We analyze two adjacent areas of the Hyblean region (SE-Sicily, Italy), a plateau that experienced Late Quaternary differential tectonic deformation. In the Floridia Basin, which recorded an almost constant background signal of regional tectonic uplift, the marine strandlines represent the key linear space-time reference lines. These are important to extrapolate the resulting age model to the laterally-correlated karst features (Fig. 11), assigned to various OISs ranging between 21 (850 ka) and 5.1 (80 ka). In contrast, in the Cassibile River basin, the paleo-sea level markers are deformed in the footwall of the Cassibile-Noto normal fault (Fig. 11). Here, in the absence of geochronological dating, we take advantage of the reconstruction of paleo-river long profiles to extrapolate the marine terrace-derived age model to the inland landforms. We thus build a 2D framework of space-time reference lines to assign ages to the paleo-karst features now abandoned and hanging along the Cassibile River valley flanks. Specifically, we attribute this karst horizon to OIS 7 (200–240 ka) and, calculate an estimated knickpoint migration rate of ~80 m ky^{-}1, allowing us to infer that karst caves exhumation occurred at ~110 ka.

Even if applied to a small area, our geomorphic approach has wider applicability to other tectonically deformed regions, especially where there is limited access to abandoned caves and/or where the infilling sediments or the occurrence of speleothems are absent or too poorly preserved for geochronology.

Supplementary data to this article can be found online at https://doi.org/10.1016/j.geomorph.2021.108095.

Declaration of competing interest

The authors declare that they have no known competing financial interests or personal relationships that could have appeared to influence the work reported in this paper.

Acknowledgement

The authors are particularly grateful to the Editor Martin Stokes for the editorial guidance and for the provided constructive comments. The authors also would like to thank Philippe Audra, Sarah Boulton and an anonymous reviewer for their helpful comments that improved the earlier version of the manuscript. This paper has been promoted by the support from the Department of Earth and Environmental Sciences of Lehigh University and from the Department of Biological, Geological and Environmental Sciences of Catania University in the frames of the "PIACERI 2020–2022 - Linea 2", scientific responsible Rosanna Maniscalco.

References

Abel, T., Hinderer, M., Sauter, M., 2002. Karst genesis of the Swabian Alb, south Germany, since the Pliocene. Acta Geol. Pol. 52 (1), 43–54.
Ambert, M., Ambert, P., 1995. Karstification des plateaux et encaissement des vallees au cours du Neogene et du Quaternaire dans les Grands Causses meridionaux (Larzac, Blandas). Geol.France 4, 37–50.
Anthony, D.M., Granger, D.M., 2007. An empirical stream power formulation for knickpoint retreat in Appalachian Plateau fluviokarst. J. Hydrol. 343, 117–126.
Antonioli, F., Kershaw, S., Renda, P., Rust, D., Belluomini, G., Cerasoli, M., Radtke, U., Silenzi, S., 2006. Elevation of the last interglacial highstand in Sicily (Italy): a benchmark of coastal tectonics. Quat. Int. 145–146, 3–18. https://doi.org/10.1016/j.quaint.2005.07.002.
Audra, P., Palmer, A.N., 2013. The vertical dimension of karst. Controls of vertical cave pattern. In: Shroder, J., Frumkin, A. (Eds.), Treatise on Geomorphology. Karst Geomorphology6. Academic Press, San Diego, pp. 186–206.
Audra, P., Palmer, A.N., 2015. Research frontiers in speleogenesis. Dominant processes, hydrogeological conditions and resulting cave patterns. Acta Carsologica 44 (3), 315–348.
Audra, P., Camus, H., Rochette, P., 2001. Le karst des plateaux jurassiques de la moyenne vallee de l'Ardeche : datations par paleomagnetisme des phases d'evolution plio-quaternaire (aven de la Combe Rajeau). Bull.Soc.Géol.France 172 (1), 121–129. https://doi.org/10.2113/172.1.121.
Bada, J.L., Belluomini, G., Bonfiglio, L., Branca, M., Burgio, E., Delitalia, L., 1991. Isoleucin epimerization ages of Quaternary mammals from Sicily. Il Quaternario 4 (1), 49–54.
Bassinot, F.C., Labeyrie, L.D., Vincent, E., Quidelleur, X., Shackleton, N.J., Lancelot, Y., 1994. The astronomical theory of climate and the age of the Brunhes-Matuyama magnetic reversal. Earth Planet. Sci. Lett. 126, 91–108.
Ben Avraham, Z., Grasso, M., 1991. Crustal structure variations and transcurrent faulting at the eastern and western margins of the eastern Mediterranean. Tectonophyisics 196, 269–277.
Ben Avraham, Z., Boccaletti, M., Cello, G., Grasso, M., Lentini, F., Torelli, L., Tortorici, L., 1990. Principali domini strutturali dalla collisione continentale neogenico-quaternaria nel Mediterraneo Centrale. Mem.Soc.Geol.Ital. 45, 453–462.
Berlin, M.M., Anderson, R.S., 2007. Modeling of knickpoint retreat on the Roan Plateau, western Colorado. J. Geophys. Res. 112, F03S06. https://doi.org/10.1029/2006JF000553.
Bhattarai, I., Gani, N.D., Xue, L., 2021. Geomorphological responses of rivers to active tectonics along the Siwalik Hills, Midwestern Nepalese Himalaya. J. Mt. Sci. 18 (5). https://doi.org/10.1007/s11629-020-6330-x.
Bianca, M., Monaco, C., Tortorici, L., Cernobori, L., 1999. Quaternary normal faulting in southeastern Sicily (Italy): a seismic source for the 1693 large earthquake. Geophys. J. Int. 139, 370–394.
Bishop, P., Hoey, T.B., Jansen, J.D., Artza, L.I., 2005. Knickpoint recession rate and catchment area: the case of uplifted rivers in eastern Scotland. Earth Surf. Process. Landf. 30, 767–778. https://doi.org/10.1002/esp.1191.
Bonforte, A., Catalano, S., Maniscalco, R., Pavano, F., Romagnoli, G., Sturiale, G., Tortorici, G., 2015. Geological and geodetic constraints on the active deformation along the northern margin of the Hyblean Plateau (SE Sicily). Tectonophysics 640–641, 80–89. https://doi.org/10.1016/j.tecto.2014.11.024.
Bosak, P., 2002. Karst processes from the beginning to the end: how can they be dated? In: Gabrovšek, F. (Ed.), Evolution of Karst: From Prekarst to Cessation. Carsologica. Založba ZRC, Postojna–Ljubljana, pp. 191–223
Bosi, C., Carobene, L., Sposato, A., 1996. Il ruolo dell'eustatismo nella evoluzione geologica nell'area mediterranea. Mem.Soc.Geol.Ital. 51, 363–382.

Boulton, S.J., 2020. Geomorphic response to differential uplift: river long profiles and knickpoints from Guadalcanal and Makira (Solomon Islands). Front. Earth Sci. 8, 10. https://doi.org/10.3389/feart.2020.00010.
Boulton, S.J., Stokes, M., 2018. Which DEM is best for analyzing fluvial landscape development in mountainous terrains? Geomorphology 310, 168–187.
Bousquet, J.C., Lanzafame, G., 2004. Compression and Quaternary tectonic inversion on the northern edge of the Hyblean Mountains, foreland of the Appenine-Maghrebian chain in eastern Sicily (Italy): geodynamic implications for Mt.Etna. GeoActa 3, 165–177.
Brocard, G.Y., Willenbring, J.K., Miller, T.E., Frederik, N.S., 2016. Relict landscape resistance to dissection by upstream migrating knickpoints. J.Geophys.Res.Earth Surf. 121, 1182–1203. https://doi.org/10.1002/2015JF003678.
Bull, W.B., 1978. Geomorphic Tectonic class of the South Front of the San Gabriel Mountains, California. U.S. Geological Survey Contract Report, 14-08-001-G-394, Office of Earthquakes. Volcanoes and Engineering, CA, Menlo Park.
Bull, W.B., McFadden, L.D., 1977. Tectonic geomorphology north and south of the Garlock fault, California. In: Dohering, D.O. (Ed.), Geomorphology in Arid Regions. Proceedings of the Eighth Annual Geomorphology Symposium. State University of New York, Binghamton, pp. 115–138.
Burollet, P.F., Mugniot, G.M., Sweeney, P., 1978. Geology of the Pelagian block: the margin and basin of Southern Tunisia and Tripolitania. In: Nairn, A., Kanes, W., Stelhi, F.G. (Eds.), The Ocean Basin And Margin. Plenum, New York, pp. 331–419.
Canora, F., Fidelibus, D., Spilotro, G., 2012. Coastal and inland karst morphologies driven by sea level stands: a GIS basedmethod for their evaluation. Earth Surf. Process. Landforms 37, 1376–1386. https://doi.org/10.1002/esp.3246.
Carbone, S., Grasso, M., Lentini, F., 1987. Lineamenti geologici del Plateau Ibleo (Sicilia S.E.): rresentazione delle carte geologiche della Sicilia Sud-Orientale. Mem.Soc.Geol. Ital. 38, 127–135.
Castillo, M., Ferrari, L., Munoz-Salinas, E., 2017. Knickpoint retreat and landscape evolution of the Amatlan de Canas half-graben (northern sector of Jalisco Block, western Mexico). J. S. Am. Earth Sci. 77, 108–122. https://doi.org/10.1016/j.jsames.2017.05.003.
Catalano, S., De Guidi, G., 2003. Late Quaternary uplift of northeastern Sicily: relation with the active normal faulting deformation. J. Geodyn. 36, 445–467.
Catalano, S., De Guidi, G., Monaco, C., Tortorici, G., Tortorici, L., 2003. Long-term behaviour of the late Quaternary normal faults in the Straits of Messina area (Calabrian arc): structural and morphological constraints. Quat. Int. 101–102, 81–91.
Catalano, S., De Guidi, G., Monaco, C., Tortorici, G., Tortorici, L., 2008a. Active faulting and seismicity along the Siculo-Calabrian rift zone. Tectonophysics 453, 177–192. https://doi.org/10.1016/j.tecto.2007.05.008.
Catalano, S., De Guidi, G., Romagnoli, G., Torrisi, S., Tortorici, G., Tortorici, L., 2008b. The migration of plate boundaries in SE Sicily: influence on the large-scale kinematic model of the African promontory in southern Italy. Tectonophysics 449, 41–62. https://doi.org/10.1016/j.tecto.2007.12.003.
Catalano, S., Romagnoli, G., Tortorici, G., 2010. Kinematics and dynamics of the late quaternary rift-flank deformation in the Hyblean Plateau (SE Sicily). Tectonophysics 486, 1–14. https://doi.org/10.1016/j.tecto.2010.01.013.
Catalano, S., Torrisi, S., Tortorici, G., Romagnoli, G., 2011. Active folding along a rift-flank: the Catania region case history (SE Sicily). J. Geodyn. 51, 53–63.
Catalano, S., Pavano, F., Romagnoli, G., Tortorici, G., 2017. Late Quaternary tectonics and active ground deformation in the Catania urban area (eastern Sicily): new constraints from a geological investigation. Tectonophysics 712–713, 200–207. https://doi.org/10.1016/j. tecto.2017.05.033.
Chappel, J., Shackleton, N.J., 1986. Oxygen isotopes and sea level. Nature 324, 137–140.
Chappell, J., Omura, A., Esat, T., McCulloch, M., Pandolfi, J., Ota, Y., Pillans, B., 1996. Reconciliation of late Quaternary sea levels derived from coral terraces at Huon Peninsula with deep sea oxygen isotope records. Earth Planet. Sci. Lett. 141, 227–236.
Colman, S.M., Pierce, K.L., 2000. Classification of Quaternary geochronologic methods. In: Noller, J.S., Sowers, J.M., Lettis, W.R. (Eds.), Quaternary Geochronology. Methods And Applications. American Geophysical Union, Washington, pp. 2–5.
Columbu, A., Chiarini, V., Waele, J.D., Drysdale, R., Woodhead, J., Helstrom, J., Forti, P., 2017. Late Quaternary speleogenesis and landscape evolution in the northern Apennine evaporite areas. Earth Surf. Process. Landf. 42 (10), 1447–1459. https://doi.org/10.1002/esp.4099.
Crosby, B.T., Whipple, K.X., 2006. Knickpoint initiation and distribution within fluvial networks: 236 waterfalls in the Waipaoa River, North Island, New Zealand. Geomorphology 82, 16–38.
De Guidi, G., Catalano, S., Monaco, C., Tortorici, L., 2003. Morphological evidence of Holocene coseismic deformation in the Taormina region (NE Sicily). J. Geodyn. 36, 193–211. https://doi.org/10.1016/S0264-3707(03)00047-4.
Despain, J.D., Stock, G.M., 2005. Geomorphic history of Crystal Cave, Southern Sierra Nevada, California. J.CaveKarst Stud. 67 (2), 92–102.
Di Grande, A., Raimondo, W., 1982. Linee di costa plio-pleistoceniche e schema litostratigrafico del Quaternario siracusano. Geol. Romana 21, 279–309.
Di Grande, A., Romeo, M., Raimondo, W., 1982. Il Membro di Gaetani` ed il Membro di Buscemi della Formazione Palazzolo: facies, distribuzione ed eta`. Boll. Soc. Geol. Ital. 101, 343–372.
Dreybrodt, W., Gabrovšek, F., 2000. Dynamics of the evolution of single karst conduits. In: Klimchouk, A.A., Ford, D.C., Palmer, A.N., Dreybrodt, W. (Eds.), Speleogenesis. Evolution of Karst Aquifers. Nat. Speleol. Soc., Huntsville, pp. 184–193.
Dumitru, T.A., 2000. Fission-track geochronology. In: Noller, J.S., Sowers, J.M., Lettis, W.R. (Eds.), Quaternary Geochronology. Methods And Applications. American Geophysical Union, Washington, pp. 131–155.
Dumitru, O.A., Polyak, V.J., Asmerom, Y., Onac, B.P., 2021. Last interglacial sea-level history from speleothems: a global standardized database. Earth Syst. Sci. Data 13 (2077–2094), 2021. https://doi.org/10.5194/essd-13-2077-2021.
Dutton, A., Scicchitano, G., Monaco, C., Desmarchelier, J.M., Antonioli, F., Lambeck, K., Esat, T.M., Fifield, L.K., Mcculloch, M.T., Mortimer, G., 2009. Uplift rates defined by U-series and 14C ages of serpulid-encrusted speleothems from submerged caves near Siracusa, Sicily (Italy). Quat. Geochronol. 4 (1), 2–10. https://doi.org/10.1016/j.quageo.2008.06.003.
Engel, J., et al., 2020. Using speleothems to constrain late Cenozoic uplift rates in karst terranes. Geology 48, 755–760. https://doi.org/10.1130/G47466.1.
Ferranti, L., Antonioli, F., Mauz, B., Amorosi, A., Dai Pra, G., Mastronuzzi, G., Monaco, C., Orrù, P., Pappalardo, M., Radtke, U., Renda, P., Romano, P., Sansò, P., Verrubbi, V., 2006. Markers of the last interglacial sea level high stand along the coast of Italy: tectonic implications. Quat. Int. 145–146, 30–54. https://doi.org/10.1016/j.quaint.2005.07.009.
Flint, J.J., 1974. Stream gradient as a function of order, magnitude, and discharge. Water Resour. Res. 10, 969–973.
Florea, L.J., Vacher, H.L., 2006. Cave Levels, Marine Terraces, Paleoshorelines, and the Water Table in Peninsular Florida. Archives of Climate Change in Karst. Geography/Geology Faculty Publications, pp. 188–192. http://digitalcommons.wku.edu/geog_fac_pub/5.
Ford, D.C., Williams, P.W., 1989. Karst Geomorphology And Hydrology. Unwin Hyman, London.
Ford, D.C., Williams, P.W., 2007. Karst Hydrogeology And Geomorphology. John Wiley & Sons Ltd., Chichester, p. 562.
Forman, S.L., Pierson, J., Lepper, K., 2000. Luminescence dating. In: Noller, J.S., Sowers, J.M., Lettis, W.R. (Eds.), Quaternary Geochronology. Methods And Applications. American Geophysical Union, Washington, pp. 157–176.
Gallen, S.F., Wegmann, K.W., Bohenstiehl, D.R., 2013. Miocene rejuvenation of topographic relief in the southern Appalachains. GSA Today 23. https://doi.org/10.1130/GSATG163A.1.
Geyh, M.A., Schleicher, H., 1990. Absolute Age Determination. Springer, Berlin.
Ghisetti, F., Vezzani, L., 1980. The structural features of the Hyblean Plateau and the Mount Judica area (South-Eastern Sicily): a microtectonic contribution to the deformational history of the Calabrian Arc. Boll.Soc.Geol.Ital. 99, 55–102.
Granger, D., Fabel, D., Palmer, A.N., 2001. PliocenePleistocene incision of the Green River, Kentucky, determined from radioactive decay of 26Al and 10Be in Mammoth Cave sediments. Geol. Soc. Am. Bull. 113 (7), 825–836. https://doi.org/10.1130/0016-7606(2001)113<0825:PPIOTG>2.0.CO;2.
Grasso, M., Reuther, C.D., 1988. The western margin of the Hyblean Plateau: a neotectonic transform system on the SE Sicilian foreland. Ann.Tecton. 2 (2), 107–120.
Guifang, Y., Xujiao, Zh., Mingzhong, T., Yamin, P., Anze, C., Zhiliang, G., Zhiyun, N., Zhen, Y., 2011. Geomorphological and sedimentological comparison of fluvial terraces and karst caves in Zhangjiajie, northwest Hunan, China: an archive of sandstone landform development. Environ. Earth Sci. 64, 671–683. https://doi.org/10.1007/s12665-010-0887-6.
Hack, J.T., 1957. Studies of longitudinal stream profiles in Virginia and Maryland. U.S. Geological Survey Professional Paper, 294-B, pp. 45–97.
Hancock, G.S., Anderson, R.S., Whipple, K.X., 1998. Beyond power: bedrock river incision process and form. In: Tinkler, K.J., Wohl, E.E. (Eds.), Rivers Over Rock: Fluvial Processes in Bedrock Channels. Geophysical Monograph Series107. AGU, Washington, D. C, pp. 35–60.
Harmand, D., Lejeune, O., Jaillet, S., Allouc, J., Occhietti, S., Brulhet, J., Fauvel, P.J., Hamelin, B., Laurain, M., Le Roux, J., Marre, A., Pons-Branchu, E., Quinif, Y., Devos, A., 2004. Dynamique de l'erosion dans le Barrois et le Perthois: incision et karstification dans les bassins-versants de la Marne, la Saulx et l'Ornain. Quaternaire 15 (4), 305–318.
Harmand, D., Adamson, K., Rixhon, G., Jaillet, S., Losson, B., Devos, A., Hez, G., Calvet, M., Audra, P., 2017. Relationships between fluvial evolution and karstification related to climatic, tectonic and eustatic forcing in temperate regions. Quat. Sci. Rev. 166, 38–56. https://doi.org/10.1016/j.quascirev.2017.02.016.
Hauselmann, P., Mihevc, A., Pruner, P., Horacek, I., Cermak, S., Hercman, H., Sahy, D., Fiebig, M., Hajna, N.Z., Bosak, P., 2015. Snezna jama (Slovenia): interdisciplinary dating of cave sediments and implication for landscape evolution. Geomorphology 247, 10–24. https://doi.org/10.1016/j.geomorph.2014.12.034.
Hayakawa, Y., Matsukura, Y., 2003. Recession rates of waterfalls in Boso Peninsula, Japan, and a predictive equation. Earth Surf. Process. Landf. 28, 675–684.
Howard, A.D., 1994. A detachment-limited model of drainage basin evolution. Water Resour. Res. 30 (7), 2261–2285.
Howard, A.D., Kerby, G., 1983. Channel changes in badlands. Geol. Soc. Am. Bull. 94, 739–752.
Hromas, J., 1968. New discoveries in Koněpruské Caves in the Bohemian Karst. Československ. kras 20, 51–62.
Jaiswara, N.K., Pandey, P., Pandey, A.K., 2019. Mio-Pliocene piracy, relict landscape and drainage reorganization in the Namcha Barwa syntaxis zone of eastern Himalaya. Sci.Rep. 9, 17585. https://doi.org/10.1038/s41598-019-54052-x.
Keller, E.A., 1986. Investigation of active tectonics: use of surficial earth processes. In: Wallace, R.E. (Ed.), Active Tectonics, Studies in Geophysics. National Academy Press, Washington, DC, pp. 136–147.
Keller, E.A., Pinter, N., 2002. Active Tectonics: Earthquakes, Uplift And Landscape, Second edition Prentice Hall, Upper Saddle River, NJ, p. 362.
Kirby, E., Whipple, K., 2001. Quantifying differential rock-uplift rates via stream profile analysis. Geology 29 (5), 415–418.
Kirby, E., Whipple, K., 2012. Expression of active tectonics in erosional landscapes. J. Struct. Geol. 44, 54–75.
Kirby, E., Whipple, K.X., Tang, W., Chen, Z., 2003. Distribution of active rock uplift along the eastern margin of the Tibetan Plateau: inferences from bedrock river profiles. J. Geophys. Res. 108, 2217. https://doi.org/10.1029/2001JB000861.
Korpas, L., 1998. Geological model of paleokarst systems: theory and applications. Geogr. Fis. Din. Quat. 21, 41–48.

Lentini, F., Carbone, S., Grasso, M., 1984. Carta geologica della Sicilia sud-orientale, scala 1: 100.000. S.EL.CA., Firenze.
Liuzzo, L., Bono, E., Sammartano, V., Freni, G., 2017. Long-term temperature changes in Sicily, Southern Italy. Atmos. Res. 198, 44–55. https://doi.org/10.1016/j.atmosres.2017.08.007.
Loget, N., Van Den Driessche, J., 2009. Wave train model for knickpoint migration. Geomorphology 106, 376–382.
Meschis, M., Scicchitano, G., Roberts, G.P., Robertson, J., Barreca, G., Monaco, C., Spampinato, C., Sahy, D., Antonioli, F., Mildon, Z.K., Scardino, G., 2020. Regional deformation and offshore crustal local faulting as combined processes to explain uplift through time constrained by investigating differentially uplifted Late Quaternary paleoshorelines: the Foreland Hyblean Plateau, SE Sicily. Tectonics 39, e2020TC006187. https://doi.org/10.1029/2020TC006187.
Meyer, M.C., Cliff, R.A., Spötl, C., 2011. Speleothems and mountain uplift. Geology 39 (5), 447–450. https://doi.org/10.1130/G31881.1.
Mocochain, L., Audra, P., Clauzon, G., Bellier, O., Bigot, J.-Y., Monteil, Ph., 2009. The effect of river dynamics induced by the Messinian Salinity Crisis on karst landscape and caves: example of the Lower Ardeche River (and Rhone valley). Geomorphology 106, 46–61. https://doi.org/10.1016/j.geomorph.2008.09.021.
Monaco, C., Bianca, M., Catalano, S., De Guidi, G., Tortorici, L., 2002. Sudden change in the Late quaternary tectonic regime in eastern Sicily: evidences from geological and geomorphological features. Boll. Soc. Geol. Ital. 1, 901–913.
Nastasi, C., Belfiore, V., Di Benedetto, T., 2014. Censimento degli insediamenti rupestri del bacino del fiume Cassibile (Sicilia Sud Orientale). Atti VIII Convegno Nazionale di Speleologia in Cavità Artificiali (7-8-9 Settembre 2012). Speleologia Iblea. XV, pp. 137–152.
Noller, J.S., Sowers, J.M., Lettis, W.R., 2000. Quaternary Geochronology. Methods And Applications. American Geophysical Union, Washington.
Ortega, A.I., Benito-Calvo, A., Perez-Gonzalez, A., Martín-Merino, M.A., Perez-Martínez, R., Pares, J.M., Aramburu, A., Arsuaga, J.L., Bermúdez de Castro, J.M., Carbonell, E., 2013. Evolution of multilevel caves in the Sierra de Atapuerca (Burgos, Spain) and its relations to human occupation. Geomorphology 196, 122–137. https://doi.org/10.1016/j.geomorph.2012.05.031.
Osservatorio delle Acque, 2005. Regione Siciliana - Assessorato Regionale dell'Energia e dei servizi di Pubblica Utilità. Retrieved from http://www.osservatorioacque.it.
Palmer, A.N., 1987. Cave Levels And Their Interpretation: National Speleological Society Bulletin. 49, pp. 50–66.
Palmer, A.N., 1991. Origin and morphology of limestone caves. Geol. Soc. Am. Bull. 103, 1–21. https://doi.org/10.1130/0016-7606(1991)103<0001:OAMOLC>2.3.CO;2.
Pavano, F., Gallen, S.F., 2021. A geomorphic examination of the Calabrian Forearc translation. Tectonics 40. https://doi.org/10.1029/2020TC006692.
Pavano, F., Romagnoli, G., Tortorici, G., Catalano, S., 2015. Active tectonics along the Nebrodi-Peloritani boundary in northeastern Sicily (southern Italy). Tectonophysics 659, 1–11. https://doi.org/10.1016/j.tecto.2015.07.024.
Pavano, F., Pazzaglia, F.J., Catalano, S., 2016. Knickpoints as geomorphic markers of active tectonics: a case study from northeastern Sicily (southern Italy). Lithosphere-US 8 (6), 633–648. https://doi.org/10.1130/L577.1.
Pavano, F., Romagnoli, G., Tortorici, G., Catalano, S., 2019. Morphometric evidences of recent tectonic deformation along the southeastern margin of the Hyblean Plateau (SE-Sicily, Italy). Geomorphology 342, 1–19.
Pedley, H.M., 1981. Sedimentology and palaeoenvironment of the southeast Sicilian Tertiary platform carbonates. Sediment. Geol. 28, 273–291.
Regalla, C., Kirby, E., Fisher, D., Bierman, P., 2013. Active forearc shortening in Tohoku, Japan: constraints on fault geometry from erosion rates and fluvial longitudinal profiles. Geomorphology 195, 84–98. https://doi.org/10.1016/j.geomorph.2013.04.029.
Regione Siciliana - Assessorato dei Beni Culturali e dell'Identità Siciliana - Dipartimento dei Beni Culturali e dell'Identità Siciliana, 2018. Piano Paesaggistico Ambiti 14-17 Siracusa - Schede Geotopi. http://www.regione.sicilia.it/beniculturali/dirbenicult/bca/ptpr/documentazioneTecnicaSiracusa.html. (Accessed 16 March 2018).
Rhodes, E.J., 1996. ESR dating of tooth enamel. In: Basile, B., Chilardi, S. (Eds.), Siracusa-le Ossa dei Giganti. Arnaldo Lombardi, Siracusa, pp. 39–44.
Rigo, M., Barberi, F., 1959. Stratigrafia pratica applicata in Sicilia. Boll.Serv.Geol.Ital. 80, 1–98.
Robustelli, G., 2019. Geomorphic constraints on uplift history in the Aspromonte Massif, southern Italy. Geomorphology 327, 319–337. https://doi.org/10.1016/j.geomorph.2018.11.011.
Rohling, E.J., Foster, G.L., Grant, K.M., Marino, G., Roberts, A.P., Tamisiea, M.E., Williams, F., 2014. Sea-level and deep-sea-temperature variability over the past 5.3 million years. Nature 508 (7497), 477–482. https://doi.org/10.1038/nature13230.
Roure, F., Howel, D.G., Muller, C., Moretti, I., 1990. Late Cenozoic subduction complex of Sicily. J. Struct. Geol. 12, 259–266.
Ruggieri, R., Maniscalco, R., Grasso, M., 2007. Variazioni eustatiche pleistoceniche e carsismo nell'area del Graben dell'Anapo (Sicilia SE). Atti del 2° Seminario Internazionale di Studi sul Carsismo negli Iblei e nell'area Sud Mediterranea. Speleologia Iblea 12, 53–60.
Schwanghart, W., Scherler, D., 2014. Short communication: TopoToolbox 2 - MATLAB-based software for topographic analysis and modelling in Earth surface sciences. Earth Surf.Dyn. 2, 1–7. https://doi.org/10.5194/esurf-2-1-2014.
Schwanghart, W., Scherler, D., 2017. Bumps in river profiles: uncertainty assessment and smoothing using quantile regression techniques. Earth Surf.Dyn. 5, 821–839. https://doi.org/10.5194/esurf-5-821-2017.
Scicchitano, G., Antonioli, F., Castagnino Berlinghieri, E.F., Dutton, A., Monaco, C., 2008. Submerged archaeological sites along the Ionian Coast of south-eastern Sicily and implications with the Holocene relative sea level change. Quat. Res. 70, 26–39. https://doi.org/10.1016/j.yqres.2008.03.008.
Serpelloni, E., Vannucci, G., Pondrelli, S., Argnani, A., Casula, G., Anzidei, M., Baldi, P., Gasperini, I., 2007. Kinematics of the Western Africa-Eurasia plate boundary from focal mechanisms and GPS data. Geophys. J. Int. 169 (3), 1–20. https://doi.org/10.1111/J.1365-246X.2007.03367.x.
Siddall, M., Rohling, E.J., Almogi-Labin, A., Hemleben, C., Meischner, D., Schmelzer, I., Smeed, D.A., 2003. Sea-level fluctuations during the last glacial cycle. Nature 423 (6942), 853–858. https://doi.org/10.1038/nature01690.
Silverman, B.W., 1986. Density Estimation for Statistics And Data Analysis. Chapman and Hall, New York.
Snyder, N.P., Whipple, K.X., Tucker, G.E., Merritts, D.J., 2000. Landscape response to tectonic forcing: digital elevation model analysis of stream profiles in the Mendocino triple junction region, northern California. Geol. Soc. Am. Bull. 112, 1250–1263.
Spampinato, C.R., Costa, B., Di Stefano, A., Monaco, C., Scicchitano, G., 2011. The contribution of tectonics to relative sea-level change during the Holocene in coastal south-eastern Sicily: new data from boreholes. Quat. Int. 232, 214–227. https://doi.org/10.1016/j.quaint.2010.06.025.
Springer, G.S., Poston, H.A., Hardt, B., Rowe, H.D., 2015. Groundwater lowering and stream incision rates in the Central Appalachian Mountains of West Virginia, USA. Int. J. Speleol. 44 (1), 99–105. https://doi.org/10.5038/1827-806X.44.1.9.
Stock, G.M., Granger, D.E., Sasowsky, I.D., Anderson, R.S., Finkel, R.C., 2005. – Comparison of U-Th, paleomagnetism, and cosmogenic burial methods for dating caves: Implications for landscape evolution studies. Earth Planet. Sci. Lett. 236, 388–403. https://doi.org/10.1016/j.epsl.2005.04.024.
Szanyi, G., Surányi, G., Leél-Össy, S., 2012. Cave development and Quaternary uplift history in the Central Pannonian Basin derived from speleothem ages. Quat. Geochronol. 14, 18–25.
Tassy, A., Mocochain, L., Bellier, O., Braucher, R., Gattacceca, J., Bourles, D., 2013. Coupling cosmogenic dating and magnetostratigraphy to constrain the chronological evolution of peri-Mediterranean karsts during the Messinian and the Pliocene: example of Ardeche Valley, Southern France. Geomorphology 189, 81–92. https://doi.org/10.1016/j.geomorph.2013.01.019.
Tortorici, G., Bianca, M., De Guidi, G., Monaco, C., Tortorici, L., 2003. Fault activity and marine terracing in the Capo Vaticano area (southern Calabria) during the Middle-Late Quaternary. Quat. Int. 101–102, 269–278.
Waelbroeck, C., Labeyrie, L., Michel, E., Duplessy, J.C., McManus, J.F., Lambeck, K., Balbon, E., Labracherie, M., 2002. Sea-level and deep water temperature changes derived from benthic foraminifera isotopic records. Quat. Sci. Rev. 21 (1–3), 295–305. https://doi.org/10.1016/S0277-3791(01)00101-9.
Wang, F., Li, H., Zhu, R., Qin, F., 2004. Late Quaternary downcutting rates of the Qianyou River from U/Th speleothem dates, Qinling mountains, China. Quat. Res. 62, 194–200. https://doi.org/10.1016/j.yqres.2004.06.007.
Wegmann, K.W., Pazzaglia, F.J., 2002. Holocene strath terraces, climate changes, and active tectonics: the Clearwater River Basin, Olympic Peninsula, Washington State. Geol. Soc. Am. Bull. 114 (6), 731–744.
Westaway, R., 1993. Quaternary uplift of southern Italy. J. Geophys. Res. 98, 21741–21772.
Whipple, K.X., 2004. Bedrock rivers and the geomorphology of active orogens. Annu.Rev. EarthPlanet.Sci. 32, 151–185.
Whipple, K.X., Tucker, G.E., 1999. Dynamics of the stream power river incision model.Implications for height limits of mountain ranges, landscape response timescales and research needs. J. Geophys. Res. 104, 17661–17674.
Whipple, K.X., Hancock, G.S., Anderson, R.S., 2000. River incision into bedrock: mechanics and relative efficacy of plucking, abrasion, and cavitation. Geol. Soc. Am. Bull. 112 (30), 490–503.
White, W.B., 1988. Geomorphology And Hydrology of Karst Terrains. Oxford University Press, New York.
Whittaker, A.C., Boulton, S.J., 2012. Tectonic and climatic controls on knickpoint retreat rates and landscape response times. J. Geophys. Res. 117, F02024. https://doi.org/10.1029/2011JF002157.
Whittaker, A.C., Cowie, P.A., Attal, M., Tucker, G.E., Roberts, G., 2007. Contrasting transient and steady state rivers crossing active normal faults: new field observations from the central Apennines, Italy. Basin Res. 19, 529–556.
Whittaker, A.C., Attal, M., Cowie, P.A., Tucker, G.E., Roberts, G., 2008. Decoding temporal and spatial patterns of fault uplift using transient river long profiles. Geomorphology 100, 506–526.
Wobus, C., Whipple, X.K., Kirby, E., Snyder, N., Johnson, J., Spyropolou, K., Crosby, B., Sheehan, D., 2006. Tectonics from topography: procedures, promise, and pitfalls. In: Willet, S.D., Hovius, N., Brandon, M.T., Fisher, D.M. (Eds.), Tectonics, Climate, And Landscape Evolution: Geologica Society of America Special Paper 398. Penrose Conference Series, pp. 55–74 https://doi.org/10.1130/2006.2398(04).